

# Simultaneous Inference of Past Demography and Selection from the Ancestral Recombination Graph under the Beta Coalescent

Kevin Korfmann<sup>1\*</sup>, Thibaut Sellinger<sup>1\*,2\*</sup>, Fabian Freund<sup>3,5</sup>,  
Matteo Fumagalli<sup>4</sup>, Aurélien Tellier<sup>1+</sup>

<sup>1</sup> Population Genetics, Department of Life Science Systems,  
Technical University of Munich (Liesel-Beckmann-Strasse 2, 85354 Freising, Germany)

<sup>2</sup> Department of Environment and Biodiversity, Paris Lodron University of Salzburg

<sup>3</sup> Institute of Plant Breeding, Seed Science and Population Genetics, University of Hohenheim  
(Fruwirthstrasse 21, 70599 Stuttgart, Germany)

<sup>4</sup> ~~Department~~ School of Biological and Behavioural Sciences, Queen Mary University of London  
(Mile End Road, London E1 4NS, UK)

<sup>5</sup> Department of Genetics and Genome Biology, University of Leicester  
(University Road, Leicester LE1 7RH, UK)

\* both author contributed equally and share first authorship

+ Corresponding author, aurelien.tellier@tum.de

## Abstract

The reproductive mechanism of a species is a key driver of genome evolution. The standard Wright-Fisher model for the reproduction of individuals in a population assumes that each individual produces a number of offspring negligible compared to the total population size. Yet many species of plants, invertebrates, prokaryotes or fish exhibit neutrally skewed offspring distribution or strong selection events yielding few individuals to produce a number of offspring of up to the same magnitude as the population size. As a result, the genealogy of a sample is characterized by multiple individuals (more than two) coalescing simultaneously to the same common ancestor. The current methods developed to detect such multiple merger events do not account for complex demographic scenarios or recombination, and require large sample sizes. We tackle these limitations by developing two novel and different approaches to infer multiple merger events from sequence data or the ancestral recombination graph (ARG): a sequentially Markovian coalescent (SM $\beta$ C) and a graph neural network (GNN $_{coal}$ ). We first give proof of the accuracy of our methods to estimate the multiple merger parameter and past demographic history using simulated data under the  $\beta$ -coalescent model. Secondly, we show that our approaches can also recover the effect of positive selective sweeps along the genome. Finally, we are able to distinguish skewed offspring distribution from selection while simultaneously inferring the past variation of population size. Our findings stress the aptitude of neural networks to leverage information from the ARG for inference but also the urgent need for more accurate ARG inference approaches.

**Keywords**— kingman coalescent, beta coalescent, selective sweep, deep learning, graph neural networks, population genetics, multiple merger coalescent, sequentially markovian coalescent, ancestral recombination graph

## 1 Introduction

2 With the availability of genomes of increasing quality for many species across the tree  
3 of life, population genetics models and statistical methods have been developed to re-  
4 cover the past history of a population/species from whole genome sequence data from  
5 several individuals [87, 58, 82, 88, 85, 5, 4, 90, 43, 44]. Indeed, the inference of the past  
6 demographic history of a species, *i.e.* population expansion, contraction, or bottlenecks,  
7 extinction/colonisation, is not only interesting in its own right, but also essential to cal-  
8 ibrate genome-wide scans to detect genes under (*e.g.* positive or balancing) selection  
9 [90, 45]. A common feature of inference methods that make full use of whole genome se-  
10 quences is the underlying assumption of a Kingman coalescent process [52] to describe the  
11 genealogy distribution of a sample. The Kingman coalescent process and its properties  
12 stem from using the traditional forward-in-time Wright-Fisher (WF) model to describe  
13 the reproduction mechanism of a population. Besides non-overlapping generations, a key  
14 assumption of the neutral WF model is that an individual offspring chooses randomly (*i.e.*  
15 uniformly) its parents from the previous generation. More precisely, each chromosome  
16 chooses a parental chromosome from the previous generation. Thus, a key parameter is  
17 the distribution of the number of offspring that parents can have. In the WF model,  
18 due to the binomial sampling, the distribution of offspring number per parent is well  
19 approximated by a Poisson distribution with both mean and variance equal to one. This  
20 implies that parents will most likely have zero, one, or two offspring individuals, but it is  
21 improbable that one parent would have many offspring individuals (*i.e.* on the order of  
22 the population size, under the Wright-Fisher haploid model the probability for a parent  
23 to have 10 or more offspring is  $\approx 10^{-8}$ ). The assumption of small variance in offspring  
24 distribution between individual parents is realistic for species with low juvenile mortality  
25 (so-called type I and II survivorship in ecology, [see survivorship curves e.g. by \[23\]](#)), such  
26 as mammals.

27 As genome sequence data become available for a wide variety of species with different  
28 biological traits and/or life cycles, the applicability of the Kingman coalescent relying on  
29 the WF model can be questioned [89, 2, 3, 69, 46, 66, 92, 63, 32]. Indeed, for some species,  
30 such as fish, with high fecundity and high juveniles mortality (type III survivorship, [\[23\]](#)  
31 ), it is expected that the variance in reproduction between parents can be much larger  
32 than under the Poisson distribution [92]. This effect is termed as sweepstake reproduction  
33 [37, 2]. Neutral processes such as strong seed banking [12], high fecundity with skewed  
34 offspring distribution [37, 27], extremely strong and recurrent bottlenecks [9, 21], and  
35 strong selective processes (*i.e.* positive selection) [26, 17, 18, 36, 3] are theoretically  
36 shown to deviate from the classic WF model in a way that the genealogies can no longer  
37 be described by a Kingman coalescent process. Under such conditions, a new class of  
38 processes arise to describe the genealogy distribution, a class where multiple individuals  
39 can coalesce and/or multiple distinguished coalescence events can occur simultaneously  
40 [78, 65, 25, 77, 71, 14]. Generally, this class of genealogical processes is called the Multiple  
41 Merger Coalescent (MMC). MMC models are more biologically appropriate than the  
42 Kingman coalescent to study many species of fish [28, 2, 3, 37], invertebrates (insects,  
43 crustaceans, etc.), viruses [61], bacteria [63, 67], plants and their pathogens [92]. While  
44 we would like to assess which population model best describes the species genealogy, field  
45 experiments to quantify the underlying reproduction mechanism of a species can be costly  
46 and time consuming at best, or intractable at worst. Therefore, an alternative solution

47 is to use inference methods based on genome data to identify which model best describes  
 48 the genealogy of a given species/population.

49 In this study we use the so-called  $\beta$ -coalescent, a specific class of MMC models.  
 50 Unlike under the WF model, under MMC models the ploidy level strongly affects the  
 51 distribution of genealogies [8]. For simplicity, in this study we focus on haploid organ-  
 52 isms. In the polyploid case, where each parent contributes multiple genomes, the SMC  
 53 formulations of putative intra- and inter-individual coalescence events would need to be  
 54 carefully modelled, since this effect would lead to smaller coalescence probabilities and a  
 55 change of the predicted statistical power for demographic inference. It is demonstrated  
 56 that if the probability of a parent to have  $k$  or more offspring is proportional to  $k^{-\alpha}$ , where  
 57  $1 < \alpha < 2$ , then the genealogy can be described by a  $\Lambda$ -coalescent [84]. The latter is a  
 58 general class of coalescent process describing how and how fast ancestral lineages merge  
 59 [71, 77]. When using the Beta( $2\alpha, \alpha$ ) distribution as a probability measure for the  $\Lambda$ -  
 60 coalescent, the transition rates (*i.e.* coalescent rate) can be analytically obtained leading  
 61 to the  $\beta$ -coalescent, a specific MMC model. If  $\alpha$  tends to 2, then the coalescent process  
 62 converges to a Kingman coalescent (up to a scaling constant): the effective population size  
 63 calculations for the Beta coalescent yield  $N_e = \frac{\mu_{\text{estimated}}}{\mu_{\text{real}}} / \text{scaling constant}^{\frac{1}{\alpha-1}}$ , where  
 64  $m = 1 + \frac{1}{2\alpha-1(\alpha-1)}$ ,  $\text{scaling constant} = \frac{(m^\alpha)}{(\alpha\beta(2-\alpha, \alpha))}$  and  $\mu_{\text{estimated}} = \frac{\theta}{(2 \cdot \sum_{i=1}^m \frac{1}{i}) \cdot L}$  [8, 55,  
 65 56]. If  $\alpha$  tends to one, the model tends to a Bolthausen-Sznitman coalescent process  
 66 (*i.e.* dominated by strong multiple merger events) [14]. The  $\beta$ -coalescent has the prop-  
 67 erty that the observed polarized Site Frequency Spectrum (SFS) of a sample of single  
 68 nucleotide polymorphisms (SNPs) exhibits a characteristic U-shape with an excess of  
 69 rare and high frequency variants (compared to the Kingman coalescent) [81]. Current  
 70 methods to draw inference under MMC models leverage information from the summary  
 71 statistics extracted from full genome data such as Site Frequency Spectrum (SFS, or  
 72 derived summary statistics) [56, 36, 76], minor allele frequency [74] or copy number al-  
 73 teration [46]. It is shown that the SFS is robust to the effect of recombination [56, 74]  
 74 and its shape allows to discriminate between simple demographic models (population ex-  
 75 pansion or contraction) under the Kingman coalescent and MMC models with constant  
 76 population size [56, 55, 28]. However, methods relying on genome-wide SFS have two  
 77 main disadvantages. First, in absence of strong prior knowledge, they can suffer from  
 78 non-identifiability [43] as several complex neutral demographic and/or selective models  
 79 under the Kingman or MMC models can generate similar SFS distributions. Second, as  
 80 they summarize the collection of underlying genealogies, they require high sample sizes  
 81 ( $>50$ ) to produce trustworthy results [56, 55, 28], relying on experimental designs which  
 82 are prohibitive for the study of non-model species. To tackle these limitations, we develop  
 83 two methods that integrate recombination events along the genome in order to leverage  
 84 more information from full genome data, thus requiring fewer samples.

85 In species undergoing sexual reproduction, recombination events break the genealogy  
 86 of a sample at different position of the genome (*i.e.* the genealogy of a sample varies along  
 87 the genome), leading to what is called the Ancestral Recombination Graph (ARG) [40, 8].  
 88 Because all the genealogical information is contained in the ARG, in this study we aim  
 89 at the interpretation of the ARGs to recover model parameters in presence of multiple  
 90 merger events. With the development of the sequentially Markovian coalescent theory  
 91 [62, 60, 98], it becomes tractable to integrate linkage disequilibrium over chromosomes

92 in inferences based on the Kingman coalescent [58]. Hence, we first develop an SMC  
93 approach based on the  $\beta$ -coalescent named the Sequentially Markovian  $\beta$  Coalescent  
94 (SM $\beta$ C). The  $\beta$ -coalescent has the additional property that, under recombination, long  
95 range dependency can be generated between coalescent trees along the genome if multiple-  
96 merger events happen in a single generation [8]. In other words, coalescent trees which  
97 are located at different places in the genome, and expected to be unlinked from one  
98 another [68], would show non-zero correlation in their topology and coalescent times.  
99 This is because coalescent trees from different genomic regions may all be affected by  
100 the same MMC event (merger event of multiple lineages in the past) which then leaves  
101 traces in the genome at several loci [9]. To overcome the theoretically predicted non-  
102 Markovian property of the distribution of genealogies along the genome under the  $\beta$ -  
103 coalescent with recombination [8] [and the increasing sparsity of genealogies and ancestral](#)  
104 [nodes with respect to  \$\alpha\$  \(see Supplementary Figure S18, S19 and S20\)](#), we develop a  
105 second method based on deep learning (DL) trained from efficient coalescent simulations  
106 [7]. In evolutionary genomics, DL approaches trained by simulations are shown to be  
107 powerful inference tools [87, 54]. Previous work demonstrated that DL approach can  
108 help overcome problems mathematically insolvable or computationally intractable in the  
109 field of population genetics [87, 6, 96, 101, 31, 22, 72, 19, 42]. The novelty of our neural  
110 network relies on its structure (Graph Neural Network, GNN) and its training algorithm  
111 based on the ARG of a sample, or its tree sequence representation [47]. GNNs are an  
112 emerging category of DL algorithm [16, 99, 20, 104] that benefit by using irregular domain  
113 data (*i.e.* graphs). GNNs are designed for the prediction of node features [53, 100], edge  
114 features (link prediction) [103, 83], or additional properties of entire graphs [102, 57].  
115 Therefore, GNNs represent a new tool to address the large dimensionality of ARGs,  
116 while simultaneously leveraging information from the genealogy (namely topology and  
117 age of coalescent events) as a substantial improvement over convolutions of genotype  
118 matrices, as currently done in the field [79].

119 We first quantify the bias of previous SMC methods (MSMC and MSMC2 [82, 95])  
120 when performing inference of past population size variation under the  $\beta$ -coalescent. We  
121 then describe our two methods, SM $\beta$ C and GNN $coal$ , and demonstrate their statisti-  
122 cal power as well as their respective limitations. From simulated tree-sequence (*i.e.*  
123 ARG) and sequence (*i.e.* SNPs) data, we assess the accuracy of both approaches to re-  
124 cover the past variation of population size and the  $\alpha$  parameter of the Beta-distribution.  
125 This parameter indicates how frequent and strong multiple merger events occur ([see](#)  
126 [Supplementary Figure S20](#)). We demonstrate that our approaches can infer the evolu-  
127 tionary mechanism responsible for multiple merger events and distinguish local selection  
128 events from genome-wide effects of multiple mergers. We highlight the limits of the  
129 Markovian property of SMC to describe data generated under the  $\beta$ -coalescent. Finally,  
130 we show that both our approaches can model and identify the presence of selection along  
131 the genome while simultaneously accounting for non-constant population size, recombi-  
132 nation, and skewed offspring distribution. Thus our methods represents a major and  
133 necessary leap forward in the field of population genetic inferences.

## 134 Materials and Methods

135 In our study we first assume the true ARG to be known. Hence, the ARG of the sample is  
 136 given as input to our methods to estimate recover model parameters of interest (*e.g.* the  $\alpha$   
 137 parameter and/or the past variation of population size). We then show the applicability  
 138 of our methods by using as input simulated sequence data (*i.e.* SNPs) and/or ARG  
 139 inferred using ARGweaver [73] from simulated sequence data.

### 140 SMC-based method

141 In this study, we use different SMC-based algorithms: two previously published, MSMC  
 142 and MSMC2 [82, 95], and the new  $SM\beta C$ . In the latter, the software backbone stems  
 143 from our previous eSMC [85, 86] whilst the theoretical framework originates from the  
 144 MSMC algorithm [82] (see Supplementary Text S1). All approaches can either use the  
 145 ARG or sequence data as input. ~~Giving~~ Providing the ARG as input for MSMC ~~an~~ and  
 146 MSMC2 is enabled by a re-implementation included in the R package eSMC2 previously  
 147 published in [86]. It is important to mention that there are no theoretical differences in the  
 148 models ~~weather sequence Data whether~~ sequence data or ARG is inputted (see [86] and  
 149 appendix Supplementary Text S1 for details), ~~the only~~. The difference is that in one case  
 150 the hidden states are inferred from sequence data with a forward-backward algorithm,  
 151 and in the later the sequence of hidden states are directly ~~build from~~ built from reading  
 152 the inputted ARG (skipping the forward-backward algorithm). The MSMC2 algorithm  
 153 focuses on the coalescence time between two haploid samples along the genome. In the  
 154 event of recombination, there is a break in the current genealogy and the coalescence time  
 155 consequently takes a new value. A detailed description of the algorithm can be found in  
 156 [29, 95]. The MSMC algorithm simultaneously analyses multiple sequences (up to 10)  
 157 and follows the distribution of the first coalescence event in a sample of size  $n > 2$  along  
 158 the sequence based on the Kingman coalescent [52]. A detailed description of MSMC can  
 159 be found in [82].

160 Our new approach,  $SM\beta C$ , is a theoretical extension of the MSMC algorithm, simulta-  
 161 neously analyzing multiple haploid sequences and focusing on the first coalescence event  
 162 of a sample size 3 or 4. ~~The 4~~ (this parameter is named  $M$  throughout the manuscript).  
 163 We define as  $M$  the number of lineages simultaneously modeled by either approach.  
 164 Hence, the  $SM\beta C$  follows the distribution of the first coalescence event of a sample size  
 165  $M$  along sequences assuming a  $\beta$ -coalescent process. Therefore, our  $SM\beta C$  allows for  
 166 more than two ancestral lineages to join the first coalescence event, or new lineages to  
 167 join an already existing binary (or triple) coalescent event. Hence, the  $SM\beta C$  extends  
 168 the MSMC theoretical framework by adding hidden states at which more than two lin-  
 169 eages coalesce. Currently, the  $SM\beta C$  has been derived to analyze for up to 4 sequences  
 170 simultaneously (due to computational load and mathematical complexity). However the  
 171  $SM\beta C$  can handle more than  $M$  sequences by analyzing all combination of sample size  $M$   
 172 before optimizing the likelihood. The emission matrix is similar to the one of MSMC. As  
 173 in the MSMC software, the population size is assumed piece-wise constant in time and  
 174 we discretize time in 40 bins throughout this study. A detailed description of  $SM\beta C$  can  
 175 be found in Supplementary Text S1. To test and validate the theoretical accuracy of our  
 176 approach, we first study its best case convergence (introduced in [86]) which corresponds  
 177 to the model's performance when the true (exact) genealogy is given as input, *i.e.* as if

178 the hidden states are known. Additionally, we also validate the practical accuracy of the  
179  $SM\beta C$  on simulated sequence data taking the same input as the MSMC software [82], or  
180 using the inferred ARGs by ARGweaver [73]. All SMC approaches used in this manuscript  
181 are found in the R package eSMC2 (<https://github.com/TPPSellinger/eSMC2>).

## 182 **GNN<sub>coal</sub> method**

183 Inspired by results obtained from inferences based on tree sequence data [34, 86], we  
184 develop a graph neural network (GNN) taking tree sequence data as input. Our GNN  
185 is designed to infer population size along with the  $\alpha$  parameter of the Beta distribution  
186 describing the distribution of offspring production. In practice, the ARG is reshaped  
187 into a sequence of genealogies (more precisely a sequence of undirected graphs), and  
188 then given as input to the GNN (similar to what is described above for the  $SM\beta C$ ).  
189 In our analyses, we fixed the batch size to 500. This value represents the number of  
190 coalescence trees being processed before updating parameters of the neural network. As  
191 the batch size is fixed to 500, only simulations displaying at least 500 recombination  
192 events are considered for the training data sets. If more than 500 recombination events  
193 occur along the sequence, the ARG is truncated and the GNN will only take as input  
194 the first 500 genealogies and remove the rest. Thanks to the GNN architecture, the  
195 algorithm can account for the topology of the genealogy. Hence, the GNN leverages  
196 information from coalescence time and branch lengths but also from the topology of the  
197 ARG. This operation is known as a graph convolution. By doing so, the GNN is capable  
198 of learning from local features of the ARG and extract information from its complex  
199 structure. To learn from global genealogy patterns (which SMC-based methods cannot  
200 do), an additional pooling strategy is implemented as part of the network [102]. To  
201 do so, the ARG is broken into smaller ARGs (*i.e.* subgraphs) during the forward-pass  
202 step. To illustrate the GNN strategy, we visualize the compression-like process, from the  
203 coalescent trees (1) being processed by GNN<sub>coal</sub> (2,3) to the inferred variable of interest  
204 (4, 5) in Figure 1.

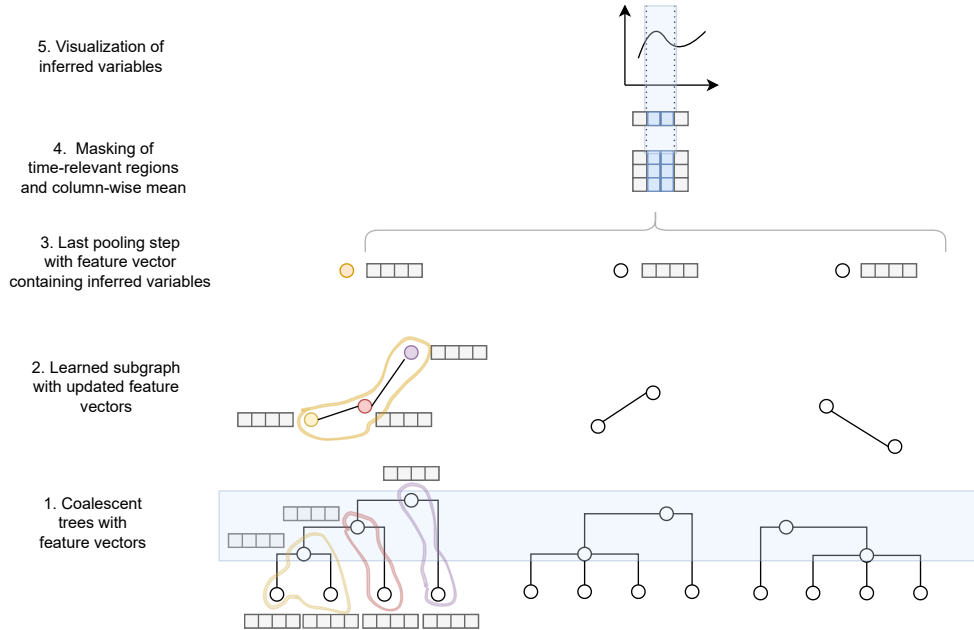


**Fig. 1. Schematic representation of  $GNN_{coal}$  processing an ARG** The figure represents the analogues compression of node embeddings (or feature vectors) as in Fig. 1 of [102]. The pooling is hierarchical and applied to each coalescent trees until a single embedding per tree remains, which is fed into a dense neural net to obtain the inferred variable of interest (*i.e.* demographic changes). Each coalescent ancestor or leaf node is initialized by this feature vector (light grey boxes) (1). Sub-graphs are generated by a pooling network with updated feature vectors and a final compression step is performed until ideally one node per graph remains (2-3). Lastly, the column-wise mean is taken after applying a time mask (blue - based on number of coalescent events), so that single feature vector remains (4-5). Detailed description of the graph convolution, feature vector initialization, pooling methodology, coalescent time mask construction, and dataset generation can be found in Supplementary Text S2 or [102].

205 To infer parameters from our neural network, we need to define an objective func-  
 206 tion to be optimized. We use a masked root-mean-squared error (RMSE) loss func-  
 207 tion as objective function which is computed for each inputted ARG (*i.e.* minimizing  
 208 the average square difference between predicted and true parameter value). In prac-  
 209 tice, time is discretized (as for the  $SM\beta C$ ) and time windows are defined. The true  
 210  $\alpha$  value and true demography at 60 predefined time points are given as input to the  
 211 GNN to compute the loss function. The GNN captures the stochastic complexity aris-  
 212 ing from the underlying demographic scenario and model parameters. Furthermore,  
 213 our algorithm naturally defines an appropriate time window to have sufficient obser-  
 214 vation at each time point. A more detailed description of the  $GNN_{coal}$  can be found in  
 215 Supplementary Text S2. The code of the model architecture is implemented in *Py-*  
 216 *torch* [70] using the extension *Pytorch Geometric* [30]. The model is available with  
 217 the simulated training dataset at <https://github.com/kevinkorfmann/GNNcoal> and  
 218 <https://github.com/kevinkorfmann/GNNcoal-analysis>.

219 **ARGweaver and tsinfer**

220 As the ARG is not known in practice, it needs to be inferred from sequence data. ARG-  
 221 weaver displays the best performance at recovering the ARG from whole genome poly-  
 222 morphism data at the sample sizes employed in this study (*i.e.*  $\ll 50$ ) [73, 15]. Briefly,

223 ARGweaver samples the ARG of  $n$  chromosomes/scaffolds conditional on the ARG of  
224  $n - 1$  chromosomes/scaffolds. To this aim, ARGweaver relies on hidden Markov models  
225 while assuming a sequentially Markov coalescent process and a discretization of time,  
226 similarly to the SMC-based methods previously described. For a more detail description  
227 of the algorithm, we refer the reader to the supplementary material of [73].

228

229 For distinguishing between MMC and selection we additionally applied tsinfer to  
230 estimate undated genealogical topologies in an effort to build a small training dataset  
231 for a model selection study reframed as classification task. Tsinfer has been chosen due  
232 to its computational performance and details about the algorithm can be found in the  
233 respective supplementary information of [48].

## 234 Simulation of data

### 235 Validation dataset for both methods

236 The ARG is given as input to the DL approach and the SM $\beta$ C (see [86]). We use msprime  
237 [7] to simulate the ARG of a sample (individuals are assumed to be haploid) under  
238 the  $\beta$ -coalescent based on [84, 8] or under the Kingman coalescent (under neutrality or  
239 selection using msprime SweepGenicSelection functionality with start and end frequency  
240 of  $1/N_e$  and 0.99, respectively). We simulate 10 sequences of 100 Mbp under five different  
241 demographic scenarios: 1) Constant population size; 2) Bottleneck with sudden decrease  
242 of the population size by a factor 10 followed by a sudden increase of population by a  
243 factor 10; 3) Expansion with sudden increase of the population size by a factor 10, 4)  
244 Contraction with sudden decrease of the population size by a factor 10; and 5) "Saw-  
245 tooth" with successive exponential decreases and increases of population size through  
246 time, resulting in continuous population size variation (as shown in [93, 82, 86]). We  
247 simulate data under different  $\alpha$  values (*i.e.* parameters of the  $\beta$ -distribution) including  
248 values of 1.9 (almost no multiple merger events), 1.7, 1.5, and 1.3 (frequent and strong  
249 multiple merger events; Supplementary Figure S20). Mutation and recombination rate  
250 (respectively  $\mu$  and  $r$ ) are set to  $10^{-8}$  per generation per bp in order to obtain the best  
251 compromise between realistic values and number of SNPs. When specified, some specific  
252 scenarios assume recombination and mutation rate set to produce sufficient data or to  
253 avoid violation of the finite site hypothesis. All python scripts used to simulate data sets  
254 are available at <https://github.com/kevinkorfmann/GNNcoal-analysis>.

255 Additionally, to generate sequence data, we simulate 10 sequences of 10 Mbp under  
256 the five different demographic scenarios described above and for the same  $\alpha$  values. For  
257 each scenario, 10 replicates are simulated. In order to obtain sufficient SNPs for inference,  
258 we simulate sequence data with mutation and recombination rate (respectively  $\mu$  and  $r$ )  
259 of  $10^{-8}$  per generation per bp when  $\alpha$  is set to 1.9 and 1.7,  $10^{-7}$  per generation per bp  
260 when  $\alpha$  is set to 1.5, and  $10^{-6}$  per generation per bp when  $\alpha$  is set to 1.3.

### 261 Training dataset for the GNN $_{coal}$

262 In our study we train two GNNs, one to infer past variation of population size through  
263 time along with  $\alpha$ , and one for model selection. The training dataset used for both GNNs  
264 is described below.



## 265 Training dataset for the GNN inferring $\alpha$ and demography

266 We generate an extensive number of ARGs to train our GNN. The ARGs are simulated  
 267 under many demographic scenarios and  $\alpha$  values. The model parameters are updated in  
 268 supervised manner. The loss function is calculated for each batch with respect to how  
 269 much the machine-learning estimates differ from to the true parameters used for sim-  
 270 ulation. The simulations strategy to recover past demographic history is based on the  
 271 strategy described and used in [13, 79]. The idea of this approach is to generate a repre-  
 272 sentative set of demographic scenarios over which the network generalizes to consequently  
 273 infer similar demographic changes after training. More details on the training strategy  
 274 can be found in Supplementary Text S2.

275 To improve the ~~outputted demographic history~~ simulated demographic history before  
 276 inference, we introduce a smoothing of the demography allowing to infer continuous  
 277 variation of population size through time. We do so by interpolating  $I$  time points  
 278 cubically, and choosing  $w$  (set to 60) uniformly spaced new time points of the interpolation  
 279 in log space. All time points more recent than ten generations in the past are discarded,  
 280 since inference is too imprecise in the very recent present under our models. An example  
 281 of this process can be seen in Supplementary Text S2.

## 282 Training dataset to disentangling coalescent and selection signatures

283 Beyond parameter inference, deep learning approaches can also be used for clustering.  
 284 Hence, we train a GNN to disentangle between different scenarios and models. In total,  
 285 we define eight classes, namely K (S0) (Kingman, no selection), K (WS) (Kingman, weak  
 286 selection), K (MS) (Kingman, medium selection), K (SS) (Kingman, strong selection) and  
 287 four different  $\beta$ -coalescent classes (~~2.0-1.75, 1.75-1.5,  $1.5 < \alpha < 2$ , 1.5-1.25,  $1.25 < \alpha < 1.5$ ,  $1.01 < \alpha < 1.25$~~ ) without selection. The three different selection  
 288 regimes are defined, ~~corresponding to  $Ne \times s$  in: 0.1, as:~~  $0.01 \leq Ne \times s < 0.1$  for SS,  $0.01$ ,  
 289  $0.001 \leq Ne \times s < 0.01$  for MS,  $0.001, 0.0001 \leq Ne \times s < 0.001$  for WS and  $Ne \times s = 0$   
 290 for absence of selection. Demography is kept constant and set to  ~~$10^5$  individuals~~  $10^4$   
 291 and  ~~$10^6$  individuals for Kingman and  $\beta$ -coalescent respectively and~~ sequence length is  
 292 set to  $10^5$  bp. The simulation is discarded if it resulted in less than 2,000 obtained trees  
 293 and is rerun with twice the sequence length until the tree number required is satisfied.  
 294 This procedure avoids simulating large genome segments of which only a small fraction  
 295 of trees is used for the given scenario during training and inference. The selection site is  
 296 introduced in the centre of the respective sequence, so that 249 trees left and 250 right of  
 297 the middle tree under selection form a training sample, using 500 trees for each sample.  
 298 One hundred replicates are generated for each training sample. The complete training  
 299 dataset consists of ~~14,000 parameter sets, 500-2,000~~ for the Kingman cases and ~~500~~  
 300 ~~2,000~~ for the  $\beta$ -coalescent cases, ~~with approximately 125 parameter sets per class (90%~~  
 301 ~~training dataset and 10% testing dataset).~~ The model itself is trained ~~on one epoch for 20~~  
 302 ~~epochs~~ (number of time the data is analyzed), and the evaluation performed ~~afterwards~~  
 303 ~~afterward~~ on 1,000 randomly generated parameter sets, with one replicate per parameter  
 304 set. ~~Branches of the datasets have been normalized by population size to avoid biases in~~  
 305 ~~the dating. Additionally, all tree sequences have been re-inferred with tsinfer to create a~~  
 306 ~~separated dataset, which has been used for training and evaluation (see results below).~~  
 307 The same architecture used for demography estimation is employed with additional linear  
 308

309 layers to reduce the number of output dimensions from 60 to 8. The loss function is set  
310 to a Cross-Entropy-Loss for the network to be trainable for categorical labels. Otherwise  
311 all architecture and training parameters is the same as described above and detailed in  
312 Supplementary Text S2.

## 313 Results

### 314 Inference bias under the wrongly assumed Kingman coalescent

315 We first study the effect of assuming a Kingman coalescent when the underlying true  
316 model is a  $\beta$ -coalescent (*i.e.* in presence of multiple merger events) by applying MSMC  
317 and MSMC2 to our simulated data. The inference results from MSMC and MSMC2  
318 when the population undergoes a sawtooth demographic scenario are displayed in Figure  
319 [2-2](#). For  $\alpha > 1.5$  the shape of the past demography is fairly well recovered. Decreasing  
320 the parameter  $\alpha$  of the  $\beta$ -coalescent (*i.e.* higher probability of multiple merger events  
321 occurring) increases the variance of inferences and flattens the demography. Yet, both  
322 methods fail to infer the correct population size, due to the scaling discrepancy between  
323 the Kingman and  $\beta$ -coalescent. Hence, we perform the same analysis and correct for  
324 the scaling effect [after the inference](#) of the MMC versus a Kingman coalescent to better  
325 capture the specific effects of assuming binary mergers only. The results are displayed in  
326 Figure S1. For  $\alpha > 1.5$  the demography is accurately recovered providing we know the  
327 true value of  $\alpha$  to adjust the y-axis (population size) scale. However, for smaller  $\alpha$  values  
328 the observed variance is extremely high and a flattened past variation of population size  
329 is observed.

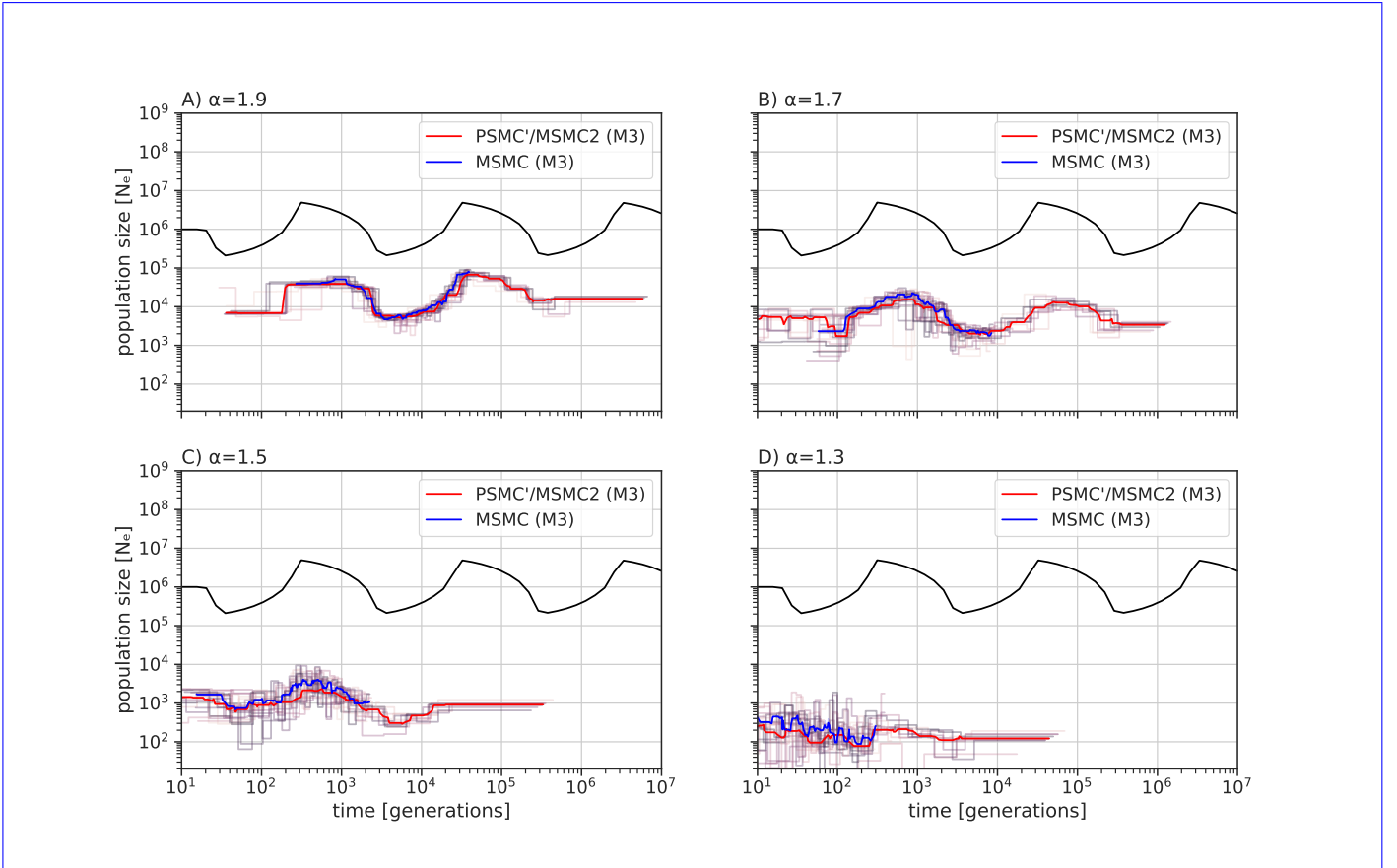


**Fig. 2. Performance of MSMC and MSMC2 under a  $\beta$ -coalescent.** Averaged estimated demographic history by MSMC (blue) and MSMC2 (red) based on 10 sequences (mean of random permutations of  $M=3$ ) of 100 Mb with  $\mu = r = 10^{-8}$  per generation per bp over ten repetitions (while analyzing simultaneously 3 sequences, noted by  $M=3$ ). Each repetition result is represented in light red (PSMC'/MSMC2) or in light blue (MSMC). Population undergoes a sawtooth demographic scenario (black) for A)  $\alpha = 1.9$ , B)  $\alpha = 1.7$ , C)  $\alpha = 1.5$ , and D)  $\alpha = 1.3$ .

### 330 The limit of the Markovian hypothesis

331 As SMC approaches rely on the hypothesis of Markovian change in genealogy along the  
 332 genome, we study the effect of  $\alpha$  on the linkage disequilibrium (LD) of pairs of SNPs  
 333 ( $r^2$ , [75, 64]) in data simulated under the Kingman Coalescent or the  $\beta$ -coalescent (with  
 334  $\alpha = 1.5$  and  $\alpha = 1.3$ ) and constant population size (Figure 3). ~~Linkage monotonously~~  
 335 ~~decreases~~ LD monotonously decreases in average with distance under the Kingman coales-  
 336 cent suggesting the hypothesis of Markovian change in genealogy to be a fair approximation  
 337 of the genealogical process in that case [97]. Under the  $\beta$ -coalescent a similar shape of  
 338 the distribution is observed but with a higher average amount of LD. We find a higher  
 339 variance in LD for smaller  $\alpha$  values. The increased variance results in the occurrence of  
 340 high spikes of LD along the genome (*e.g.* Figure 3 B). The stochastic increase of linkage  
 341 along the genome demonstrates that the Markovian hypothesis used to model genealogies  
 342 along the genome is strongly violated under the  $\beta$ -coalescent due to the long range effect  
 343 of strong multiple merger events [8].

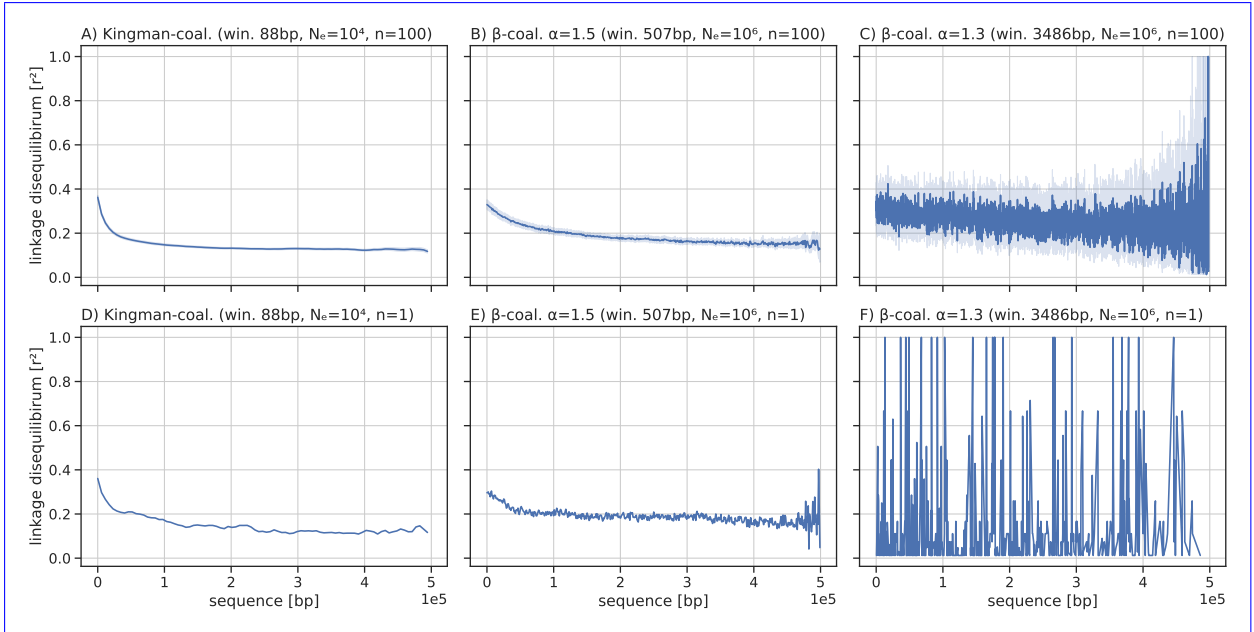


**Fig. 3. Linkage disequilibrium under a Kingman and  $\beta$ -coalescent.** Pairwise linkage disequilibrium between SNPs ( $r^2$ ) under a Kingman and  $\beta$ -coalescent with  $\alpha = 1.5$  and  $\alpha = 1.3$  using 100 sequences of length 0.5 Mb for A) - C) and 1 replicate in D) - F). The population size is constant at  $N = 10^4$  for the Kingman model and  $N = 10^6$  for the  $\beta$ -coalescent, with  $\mu = 1 \times 10^{-7}$  and  $r = 1 \times 10^{-8}$  per generation per bp. For each LD analysis, the linkage disequilibrium is calculated by averaging it over automatically-selected window sizes, such that on average at least two mutations are in each window for A) to F), respectively.

344 We further investigate the effect of multiple merger events on LD. To this aim, we  
 345 first assume an SMC framework (*e.g.* MSMC2 or eSMC) to predict the transition matrix  
 346 (*i.e.* matrix containing the probabilities for the coalescent time to change to another value  
 347 along-between two positions of the genome) and investigate the absolute difference between the observed transition events. Under the Kingman coalescent, the  
 348 distribution of coalescent times between two positions in a sample of size two ( $n = 2$ )  
 349 is well ~~approximated by the SMC as shown spread across hidden states~~ in Figure S2  
 350 (*i.e.* absence of structured difference between observed and predicted transition events).  
 351 However, under the  $\beta$ -coalescent (with  $\alpha = 1.3$ ) we observe significant ~~and~~ differences  
 352 between observed and predicted transition events at times points where multiple merger  
 353 events occur (Figure S3). ~~In practice, More precisely we observed transitions at specific~~  
 354 time points (corresponding to multiple merger events) ~~do not occur at each time point~~  
 355 ~~(as they remain rare events), unveiling a~~ occurring much more frequently than what  
 356 is predicted by the model (dark blue lines). This plot thus shows that multiple merger  
 357 events do not affect the genealogy at every time point and that multiple merger events  
 358 are over represented in the distribution of transitions events due to the long range effects  
 359 of MMC events (*i.e.* many positions of the genome contain the same information). This  
 360 means that one multiple merger coalescent events can affect all positions in the genomes  
 361 (explaining the spikes in the LD distribution). In contrast, under the Kingman coalescent  
 362 with recombination, the probability for a coalescent event to affect the whole genome is  
 363 negligible.  
 364

365 This plot thus unveils the discrepancy between the expectation from the SMC (*i.e.*  
 366 approximating the distribution of genealogies along the genome by a Markov chain) and

367 the ~~simulated data~~ actual effect of multiple merger events on the genealogy distribution  
 368 along the genome. This discrepancy does not stem from the simulator, because it correctly  
 369 generates ARG under the  $\beta$ -coalescent model [8, 7], but from the limits of the SMC  
 370 approximation to model events with long range effects on the ARG (Figure S3).

### 371 Inferring $\alpha$ and past demography on ARG

372 To test if our two approaches (GNNcoal and SM $\beta$ C) can recover the past variation of  
 373 population size and the  $\alpha$  parameter, we run both methods on simulated tree sequences  
 374 under different  $\alpha$  values and demographic scenarios. Figure 4 displays results for data  
 375 simulated under a sawtooth past demography and for  $\alpha$  ranging from 1.9, 1.7, 1.5 to  
 376 1.3. In all cases, the GNNcoal approach exhibits ~~high accuracy and~~ low variance to  
 377 infer the variation of population size and high accuracy from 1.9 to 1.5 with a noticeable  
 378 drop in accuracy for 1.3 attributable to the ever increasing sparsity due to decreasing  $\alpha$   
 379 generating stronger  $\beta$ -coalescent events. For high  $\alpha$  values ( $>1.5$ ), the shape of population  
 380 size variation is well recovered by SM $\beta$ C (4). However, for smaller values, the observed  
 381 high variance demonstrates the limits of SMC inferences.

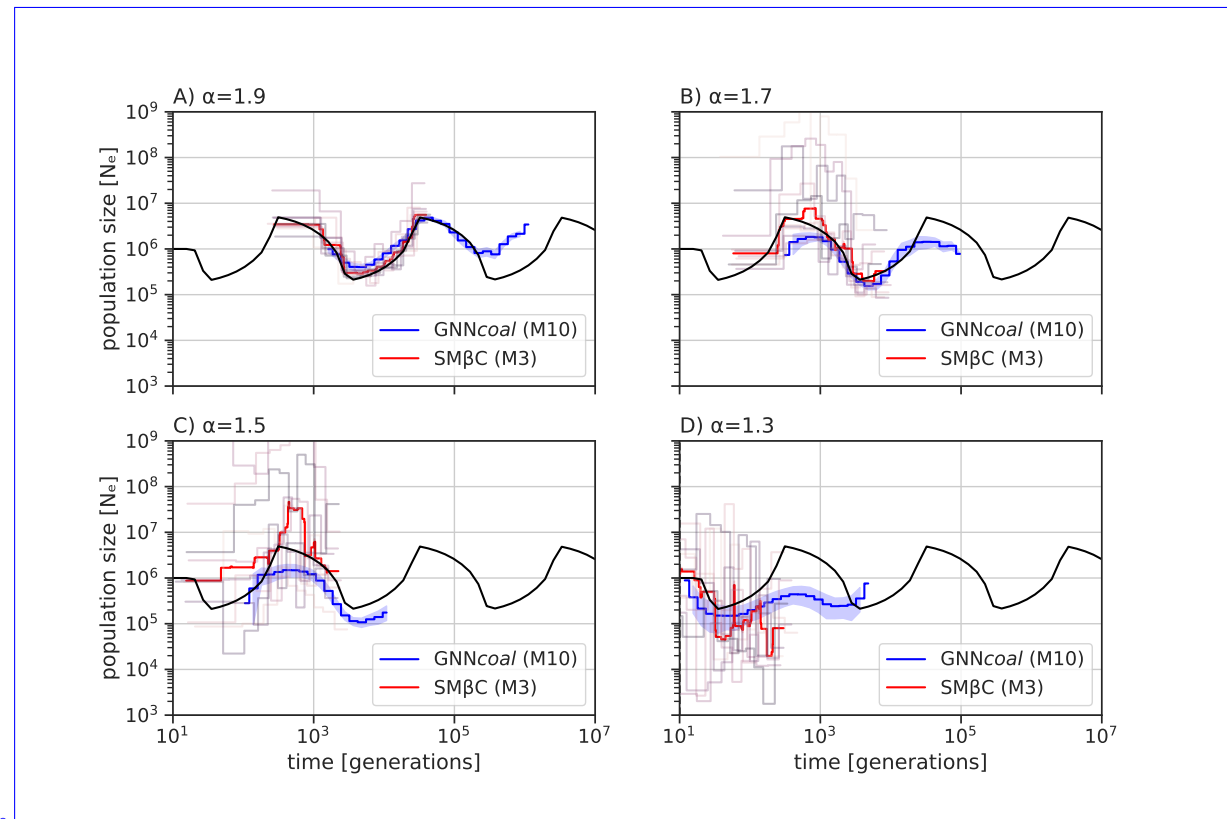


**Fig. 4. Best-case convergence estimations of SM $\beta$ C and GNNcoal under a  $\beta$ -coalescent.** Estimations of past demographic history by SM $\beta$ C in red (median) and by GNNcoal in blue (mean and 95% confidence interval, CI95; while analyzing simultaneously  $M=3$  or  $M=10$  sequences; individual replicates of SM $\beta$ C shown as light lines) when population undergoes a sawtooth demographic scenario (black) under A)  $\alpha = 1.9$ , B)  $\alpha = 1.7$ , C)  $\alpha = 1.5$  and D)  $\alpha = 1.3$ . SM $\beta$ C runs on 10 sequences and 100 Mb, GNNcoal runs on 10 sequences and 500 trees, and  $\mu = r = 10^{-8}$  per generation per bp.

382 On average, both approaches seem to recover fairly well the true  $\alpha$  value (Figure 4  
383 ~~and Table 1 in 5 and Table S1~~). In particular, *GNNcoal* displays high accuracy and  
384 lower standard deviation. We note that the variance in the estimation of  $\alpha$  increases  
385 with diminishing  $\alpha$  value. Moreover, increasing the number of simultaneously analyzed  
386 sequences by *SM $\beta$ C* does not seem to improve the inferred  $\alpha$  value (Table S1). These  
387 conclusions are also valid for the results in ~~Figures Figure~~ S4-S7 and Table S1 based on  
388 inference under four additional demographic scenarios: constant population size, bottle-  
389 neck, sudden increase and sudden decrease of population size.

390  
391 ~~Because when~~ When  $\alpha$  diminishes, the effective population size decreases and the  
392 number of recombination events plummets for small values of  $\alpha < 1.5$ . To demonstrate  
393 the theoretical convergence of *SM $\beta$ C* to the correct values, we run *SM $\beta$ C* on data simu-  
394 lated with mutation and recombination rate fifty times higher under similar scenarios as  
395 in Figure 4. This operation increases the amount of data in the form of SNPs and number  
396 of independent coalescent trees by recombination. Since branch lengths (in generations)  
397 are on average smaller in the presence of multiple merger when compared to a Kingman  
398 coalescent, we choose to increase the rates as opposed to increasing the genome lengths,  
399 which does not affect the branch lengths (but increases the number of genealogies). Re-  
400 sults of *SM $\beta$ C* for  $\alpha$  values of 1.7, 1.5 and 1.3 are displayed on Table S2. ~~Results Overall~~  
401 our results show that *SM $\beta$ C* can recover  $\alpha$  with higher accuracy when more data is avail-  
402 able. To be more precise when  $M = 3$  ( $M$  being the number of simultaneously haploid  
403 sequence analyzed), the overall average inferred  $\alpha$  values improve from 1.6, 1.53 and 1.42  
404 (Table S1) to 1.64, 1.49 and 1.36 (for data simulated respectively under  $\alpha = 1.7, \alpha = 1.5$   
405 and  $\alpha = 1.3$ ). Yet when  $M = 4$  a gain in accuracy is only observed for  $\alpha = 1.5$  and  
406  $\alpha = 1.3$ . Indeed, the overall average inferred  $\alpha$  values changed from 1.60, 1.54 and 1.47  
407 (Table S1) to 1.58, 1.47 and 1.39 (for data simulated respectively under  $\alpha = 1.7, \alpha = 1.5$   
408 and  $\alpha = 1.3$ ).

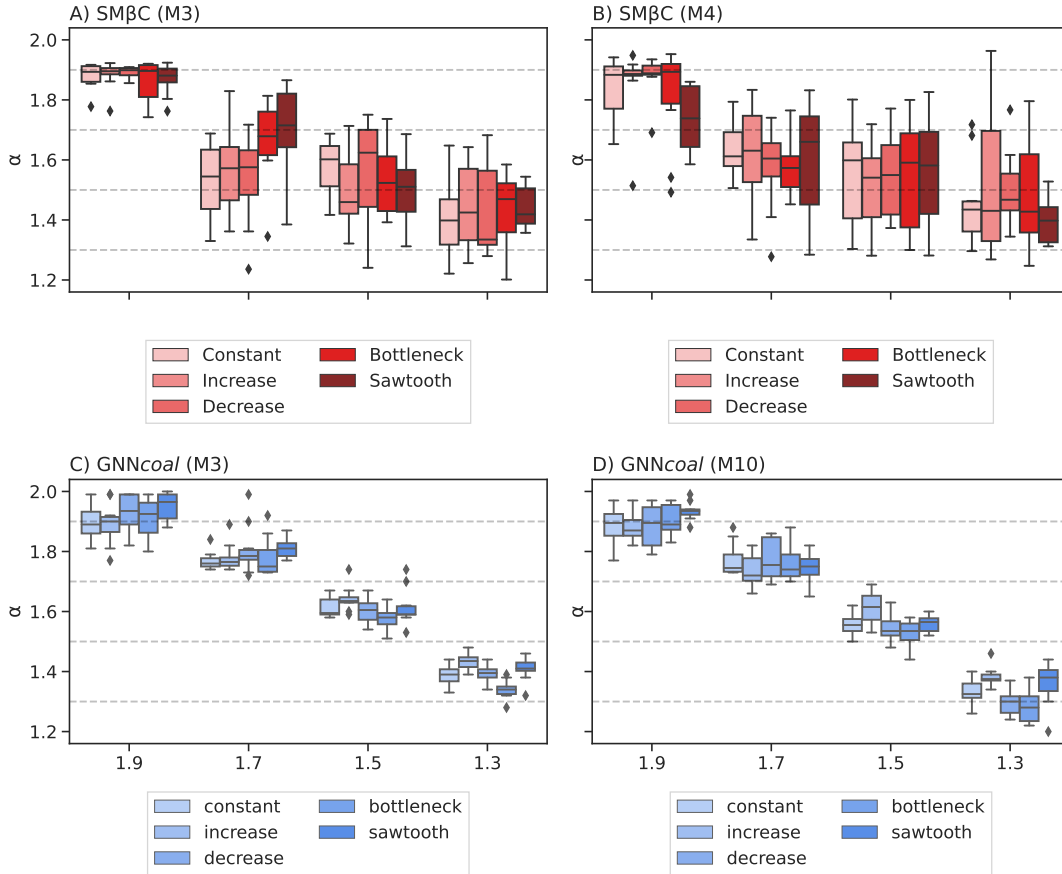


**Fig. 5. Estimated  $\alpha$  values by SM $\beta$ C and GNNcoal.** Estimated values of  $\alpha$  by SM $\beta$ C and GNNcoal over ten repetitions using 10 sequences of 100 Mb with  $\mu = r = 10^{-8}$  per generation per bp under a  $\beta$ -coalescent process (with different  $\alpha$  parameter). The analysis are run on five different demographic scenarios (Constant population size, Bottleneck, Sudden increase, Sudden decrease and a Sawtooth demography) using a sample size  $n = 3$  for A) and C),  $n = 4$  for B), and  $n = 10$  for D). Grey dashed lines indicate the true  $\alpha$  values. [For exact values and standard deviations of the respective experiment see Supplementary Table S1.](#)

409 Although 10 sequences are given to SM $\beta$ C in the previous analyses, the method can  
 410 only analyze three or four simultaneously. On the other hand, GNNcoal can simulta-  
 411 neously analyze 10 sequences, that is the whole simulated ARG. As we observe that  
 412 GNNcoal has a higher performance than SM $\beta$ C, we wish to test whether the GNNcoal  
 413 better leverages information from the ARG or benefits from simultaneously analyzing  
 414 a larger sample size. Thus, we run GNNcoal on the same dataset, but downsampling  
 415 the coalescent trees to a sample size three. Results [for sample size ten](#) are displayed in  
 416 Figure S4 to [Figure S7](#) ~~Results and downsampled results~~ with sample size three ( $M=3$ )  
 417 ~~of GNNcoal are similar to results with sample size 10,~~ [which appear to be similar, are](#)  
 418 [displayed in Figure S8](#), demonstrating that the GNNs can better leverage information  
 419 from the ARG in presence of multiple merger events([Figure S8](#)).

420 Additionally, we test if both approaches can recover a Kingman coalescent from the  
 421 ARG when data are simulated under the Kingman coalescent, namely both approach  
 422 should recover  $\alpha = 2$ . To do so, we simulate the same five demographic scenarios as above

under a Kingman coalescent and infer the  $\alpha$  parameter along with the past variation of population size. Estimations of  $\alpha$  values are provided in Table 1 and are systematically higher than 1.85, suggesting mostly binary mergers. The associated inferred demographies are shown in Figures S9-S13. Both approaches correctly infer the past demographic shape up to the scaling discrepancy between the Beta and the Kingman coalescent (as previously described). Furthermore, we notice that the scaling effect only affects the y-axis for the  $SM\beta C$  but affect both axes for  $GNNcoal$ .

As  $GNNcoal$  was not trained on data simulated under the Kingman coalescent (especially with such high population size), some events fall beyond the scope of the GNN due to the scaling discrepancy between the Beta and Kingman coalescence. Hence, we run  $GNNcoal$  on data simulated under the Kingman coalescent but with smaller population size (scaled down by a factor 100) to assure that all events fall within the scope of the GNN. Values of  $\alpha$  inferred by the  $GNNcoal$  and the  $SM\beta C$  under the five demographic scenarios are available in Table S3. The associated inference of population size are plotted in Figure S9-S12. Both approaches recover high  $\alpha$  values (*i.e.*  $>1.85$ ) suggesting a genealogy with almost exclusively binary mergers. In addition, both approaches accurately recover the shape of the past variation of population size up to a scaling constant but only on the population size y-axis.

## Inferring $\alpha$ and past demography from simulated sequence data

We first investigate results for both  $GNNcoal$  and  $SM\beta C$  ~~when the ARG is reconstructed with ARGweaver [73], the latter with the objective of evaluating the performance on ARG reconstructed from sequence data using ARGweaver [73] as ARGweaver is currently being considered the best performing approach to infer ARG for sample size smaller than 20 [15].~~ Demographic inference results by both approaches are displayed in Figure S14, and  $\alpha$  inference results in Table S4.  $GNNcoal$  does not recover the shape of the demographic history from the inferred ARGs and largely overestimates  $\alpha$ . In contrast,  $SM\beta C$  produces better inferences of  $\alpha$  when giving the inferred ARG as input when compared to the GNN.  $SM\beta C$  recovers the shape of the past variation of population size for  $\alpha > 1.3$  but displays extremely high variance for  $\alpha = 1.3$ .

~~We then run~~ We then evaluate  $SM\beta C$  on simulated sequence data to compare the necessity of reconstructing the ARG for the SMC method and found that  $\alpha$  is typically well recovered (Table 2) and that results are similar to what obtained when the true ARG is given. Furthermore, the shape of the past variation of population size is well inferred under the sawtooth demographic scenario for  $\alpha > 1.3$  (Figure S15). In the other four scenarios, the shape of the demography is recovered in recent times but population sizes are underestimated in the past (Figure S16). Finally, as found above from inputted ARGs, the variance in estimates of population sizes generally increases with diminishing  $\alpha$ .

## Inferring MMC and accounting for selection

As specific reproductive mechanisms and selection can lead to the occurrence of multiple merger-like events, we train our neural network on data simulated under the  $\beta$ -coalescent, and under the Kingman coalescent in presence or absence of selection to assess our methods capacity to distinguish between them. We then use the trained



466 GNNcoal to determine if multiple merger events originate from skewed offspring distri-  
 467 bution or positive selection, or if the data follows a neutral Kingman coalescent process.  
 468 The classification results are displayed in Figure 6 in the form of ~~a confusion matrix,~~  
 469 ~~that is confusion matrices, where~~ the percentage of times the GNNcoal correctly as-  
 470 signs the true model shown on the diagonal evaluated on a test dataset of 1,000 ~~known~~  
 471 ~~ARGs. Our approach can accurately select the model except in two cases. GNNcoal~~  
 472 ~~shows limited power to distinguish between strong and intermediate selection under the~~  
 473 ~~Kingman coalescent, as well as to distinguish between the  $\beta$ -coalescent with a small~~  
 474 ~~amount of multiple merger events (*i.e.* ARGs. We tested three scenarios A) training and~~  
 475 ~~evaluating on known exact ARGs, B) training on exact ARGs but evaluating on inferred~~  
 476 ~~ARGs, and, lastly C) training and evaluating on inferred ARGs. The results indicate~~  
 477 ~~the necessity of integrating inference errors or instances of branch unresolvability into~~  
 478 ~~the training process. The network is able of distinguishing between signals of multiple~~  
 479 ~~merger, which translate to an estimate of  $\alpha > 1.75$ ) and the~~, from simple ARG-estimation  
 480 ~~uncertainties. The overall confusion between neighboring classes may be attributed to~~  
 481 ~~the comparably small size of training data (4,000 simulations), which enabled to build a~~  
 482 ~~training dataset comprised of inferred trees within few hours. To summarize our approach~~  
 483 ~~can accurately distinguish between Kingman and  $\beta$ -coalescent case with  $1.75 > \alpha > 1.5$ , but~~  
 484 ~~uncertainty needs to be part of the training procedure.~~

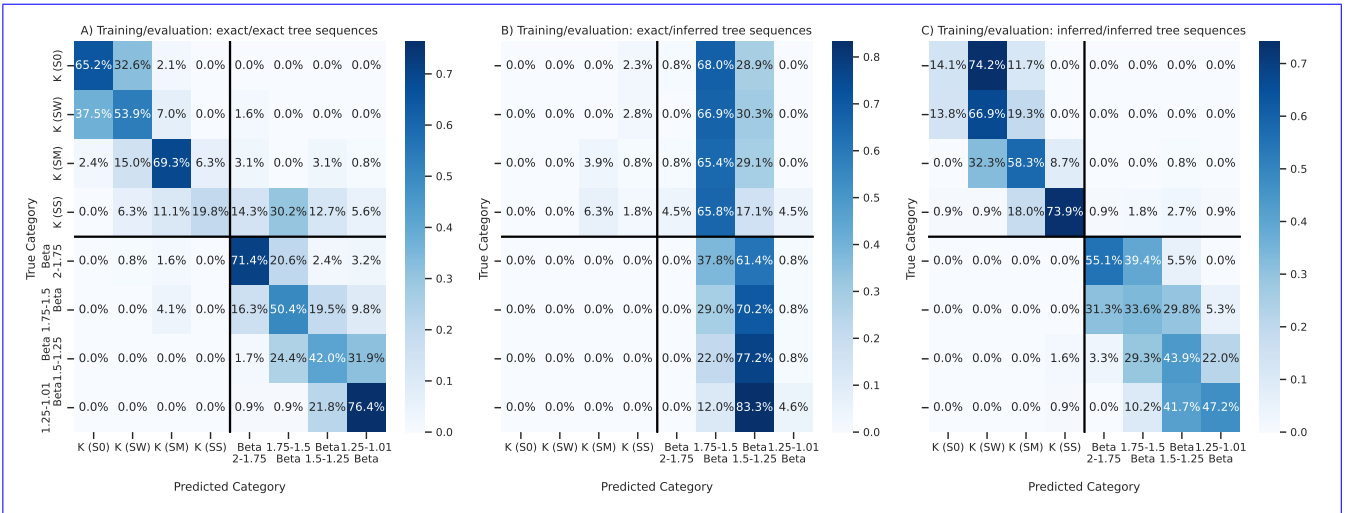


**Fig. 6. Confusion matrix for Kingman and  $\beta$ -coalescent classification model under varying selection coefficients.** Evaluation of classification accuracy for Kingman (K) and  $\beta$ -coalescent (B) for no selection (S0), weak selection (SW), medium selection (SM) and strong selection (SS) using a 1,000 repetition validation dataset (and small 4000 proof-of-concept repetition training set). Population size was kept constant at  $N = 10^4$  individuals for the Kingman scenario and at  $N = 10^6$  for the  $\beta$ -coalescent, using a sample size  $n = 10$  and  $r = 10^{-8}$  per bp per generation. Branch length are normalized by the respective population size. Classification model has been trained and evaluated either on exact or inferred tree sequences (tsinfer without dating) as indicated in the subfigure titles of A), B) and C).

485 ~~To assess the~~  
 486 ~~Since strong selection can lead to multiple merge coalescent or rapid and successive~~  
 487 ~~coalescent events (as the beneficial alleles spreads very quickly in the population) [26, 11, 76]~~  
 488 ~~, we investigate if our approaches can model and recover the effect of selection. Therefore,~~  
 489 ~~we infer  $\alpha$  along the genome (to model the local effect of selection on the genome) with~~

490 both approaches from ~~data-true genealogies~~ simulated with strong positive selection or  
 491 neutrality under a Kingman coalescent with population size being constant through time.  
 492  $SM\beta C$  infers  $\alpha$  on windows of 10kbp along the genome, and  $GNNcoal$  infers  $\alpha$  every 20  
 493 trees along the genome. Results for  $GNNcoal$  and  $SM\beta C$  are displayed in Figure 7. ~~Both~~  
 494 ~~approaches recover~~ The  $SM\beta C$  approach recovers smaller  $\alpha$  value around the locus under  
 495 strong selection (while  $GNNcoal$  displays higher variance). However under neutrality or  
 496 weak selection, inferred  $\alpha$  values remain high ( $>1.6$ ) along the genome.

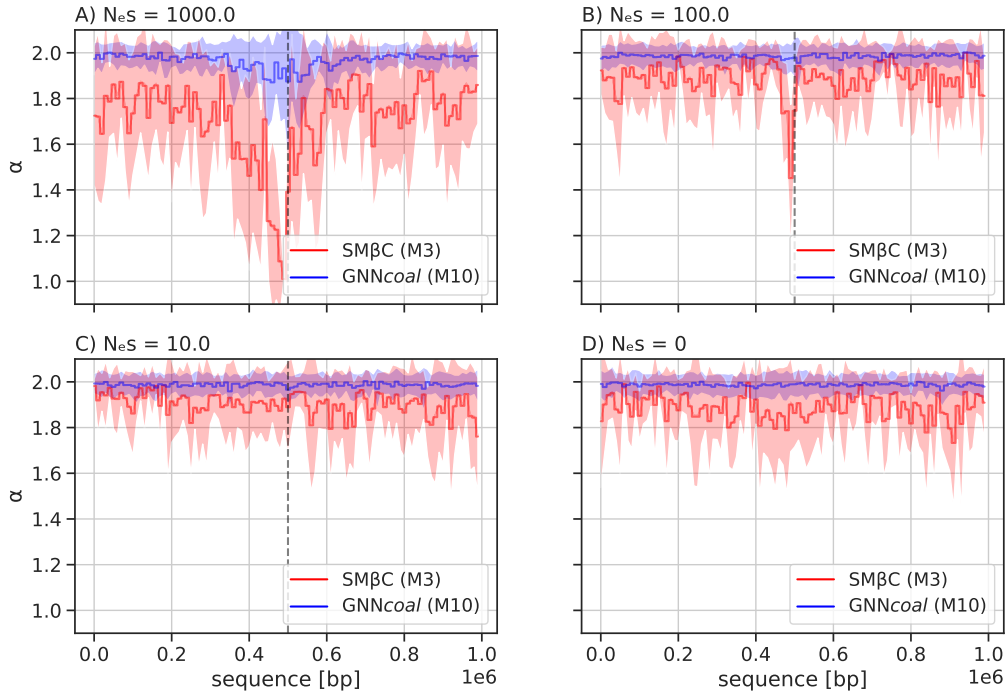


**Fig. 7. Averaged estimations by  $GNNcoal$  and  $SM\beta C$  under selection** Estimations of  $\alpha$  along the genome by the  $GNNcoal$  approach and the  $SM\beta C$  when population undergoes as strong positive selective sweep event (at position 0.5 Mb) under different strengths of selection: A)  $s = 0.01$ , B)  $s = 0.001$ , C)  $s = 0.0001$ , and D)  $s = 0$  meaning neutrality (mean and standard deviation for both methods). The population size is constant and set to  $N = 10^5$  with  $\mu = r = 10^{-8}$  per generation per bp. We hence have in A)  $N_e \times s = 1000$ , B)  $N_e \times s = 100$ , C)  $N_e \times s = 10$  and D)  $N_e \times s = 0$ .  $SM\beta C$  uses 20 sequences of 1Mb (red) and  $GNNcoal$  uses 10 sequences through down-sampling the sample nodes (blue)

497 Similarly, we run both approaches on ~~data-genealogies~~ simulated under the  $\beta$ -coalescent  
 498 (assuming neutrality) and we infer the  $\alpha$  value along the genome. Inferred  $\alpha$  values by  
 499 both approaches are plotted in Figure ~~17 in S1S17~~.  $GNNcoal$  is able to recover the  $\alpha$   
 500 value along the genome with moderate overestimation due to tree sparsity. On the con-  
 501 trary,  $SM\beta C$  systematically underestimates  $\alpha$  values. Nevertheless, unlike in presence of  
 502 positive selection at a given locus, the inferred  $\alpha$  values are found in all cases to be fairly  
 503 constant along the genome.

504 We finally simulate data under a ~~strong selective sweeps~~ Kingman coalescent (true  
 505 genealogies) with a strong selective sweep or under neutrality conditioned on a sawtooth

506 demographic scenario [to test our methods' simultaneous inference capabilities](#). Under  
 507 neutrality, our both approaches recover, as expected, high  $\alpha$  values along the genome and  
 508 can accurately recover the past variation of population size (only up to a scaling constant  
 509 for *GNNcoal*, since it was trained on the  $\beta$ -coalescent only) (Figure 8). Similarly, when  
 510 the simulated data contains strong selection, a small  $\alpha$  value is recovered at the locus  
 511 under selection and the past variation of population size is accurately recovered, albeit  
 512 with a small underestimation of population size in recent times for *SM $\beta$ C* (Figure 8).

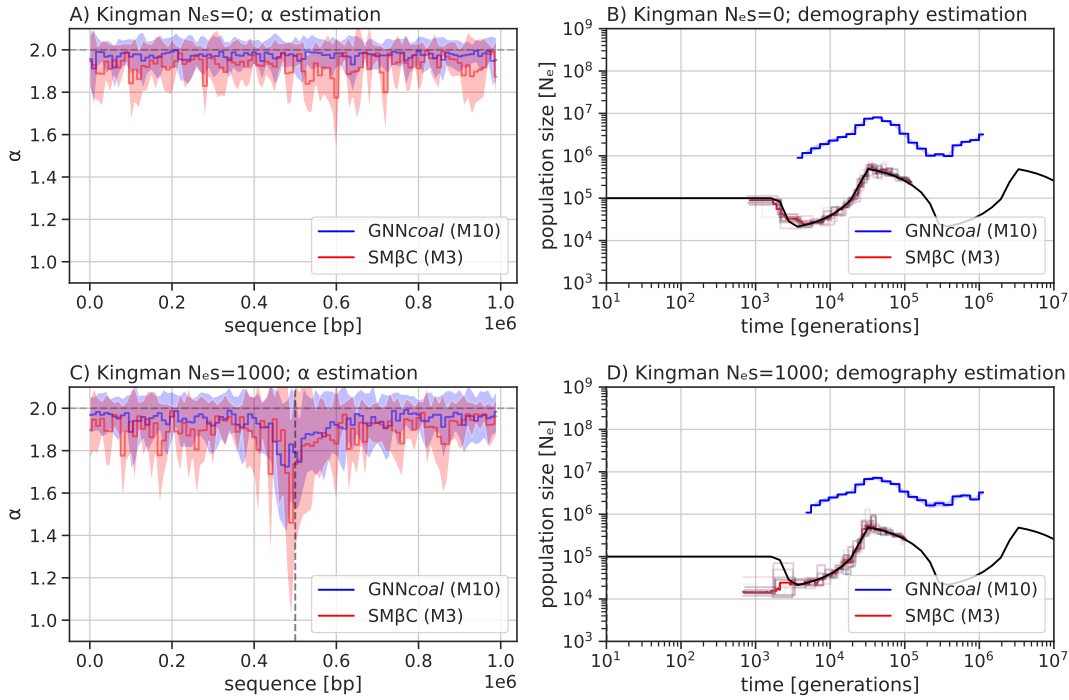


**Fig. 8. Simultaneous estimations of  $\alpha$  along the sequence under demographic change by *GNNcoal* and *SM $\beta$ C*.** Simultaneous estimation of  $\alpha$  along the genome under a partial sawtooth scenario: A) and B) in the absence of selection (mean and standard deviation for both methods), and C) and D) presence of selection with  $N_e S = 1,000$  (mean and CI95 for *GNNcoal* and median for *SM $\beta$ C*). *SM $\beta$ C* uses 20 sequences of 1Mb (red) and *GNNcoal* uses 10 sequences through down-sampling the sample nodes (blue), and  $\mu = r = 10^8$  per generation per bp.

## 513 Discussion

514 With the rise in popularity of SMC approaches for demographic inferences [58], most  
 515 current methods leverage information from whole genome sequences by simultaneously  
 516 reconstructing a portion of the ARG to infer past demographic history [58, 82, 93, 94],  
 517 migration rates [51, 95], variation in recombination and mutation along the genome [5, 4],  
 518 as well as ecological life history traits such as selfing or seed banking [85, 91]. However,  
 519 other previous studies proposed to uncouple both steps, namely by first reconstructing  
 520 the ARG and by then inferring parameters from its distribution [86, 34, 73]. Indeed,  
 521 recent efforts have been made to improve approaches to recover the ARG [88, 49, 39, 73,  
 522 59, 15], as well as its interpretation [33, 86]. Our results on data simulated under the

523  $\beta$ -coalescent clearly show the strong effect of multiple merger events on the topology and  
524 branch length of the ARG. We find that the more multiple merger events occur, the more  
525 information concerning the past demography is lost. Both *GNNcoal* and *SM $\beta$ C*, whether  
526 given sequence data, the true or inferred ARG, can recover the  $\alpha$  parameter and the  
527 variation of past population size for  $\alpha$  values high enough (*i.e.*  $\alpha > 1.3 > 1.5$ ). However,  
528 for lower values of  $\alpha$ , a larger amount of data is necessary for any inference, specifically  
529 in the form of a high effective population size (correspondingly adequate mutation and  
530 recombination rates) and sufficient sequence length, which becomes nearly impossible  
531 when  $\alpha$  tends to one. Both approaches can also recover the Kingman coalescent (*i.e.*  
532  $\alpha > 1.8$ ). We find that *GNNcoal* outperforms *SM $\beta$ C* in almost all cases when given the  
533 true ARG, and we demonstrate that *GNNcoal* can be used to disentangle between  $\beta$ -  
534 coalescent and Kingman models with selection.

535 Overall, our results provide a substantial improvement in the development of inference  
536 methods for models with multiple merger events, a key step to understand the underlying  
537 reproduction mechanism of a species. While still inferring population sizes of the correct  
538 order of magnitude, *SM $\beta$ C* is outperformed by *GNNcoal* when given true ARGs as input.  
539 As ARG inference method improve, GNN models will offer a promising alternative to  
540 current SMC methods. As we directly compare our theoretical SMC to the GNN based  
541 on the same input data (coalescent trees), we are ideally placed to dissect the mecha-  
542 nisms underlying the power of the *GNNcoal* method. We identify four main reasons for  
543 the difference in accuracy between the two methods developed. First, the *SM $\beta$ C* ap-  
544 proach suffers from the limit of the sequential Markovian coalescent hypothesis along the  
545 genome when dealing with strong multiple merger events [8, 21]. Second, most ~~of~~ current  
546 SMC approaches, except XSMC [50], rely on a discretization of the coalescent times into  
547 hidden states, meaning that simultaneous mergers of three lineages may not be easily  
548 distinguished from two consecutive binary mergers occurring over a short period ~~of time~~.  
549 Third, the *SM $\beta$ C* relies on a complex hidden Markov model and due to computational  
550 and mathematical tractability, it cannot leverage information on a whole genealogy. In  
551 fact, as MSMC, *SM $\beta$ C* only focuses on the first coalescent event, and therefore cannot  
552 simultaneously analyze large sample size. Furthermore, the *SM $\beta$ C* approach leverages  
553 information from the distribution of genealogies along the genome. Whilst, in the near  
554 absence of recombination events, both approaches cannot utilize any information from the  
555 genealogy itself, *GNNcoal* can overcome this limit by increasing the sample size. Fourth,  
556 the *SM $\beta$ C* is based on a coalescent model where  $\alpha$  is constant in time. Yet multiple  
557 merger events do not appear regularly across the genealogical timescale, but occur at  
558 few random time points. Hence, the SMC approach suffers from a strong identifiability  
559 problem between the variation of population size and the  $\alpha$  parameter (for low  $\alpha$  values).  
560 For instance, if during one hidden state one strong multiple merger event occurs, multi-  
561 ple merger events are seldom observed and *SM $\beta$ C* may rather assume a small population  
562 size at this time point (hidden state). This may explain the high variance of inferred  
563 population sizes under the  $\beta$ -coalescent.

564 By contrast, *GNNcoal* makes use of the whole ARG, and can easily scale to larger  
565 sample sizes (over 10), although it recovers  $\alpha$  with high accuracy with sample size  $M = 3$   
566 only. Our interpretation is that *GNNcoal* is able of simultaneously leveraging information  
567 from topology and the age of coalescent events (nodes) across several genealogies (here  
568 500). *GNNcoal* ultimately leverages information from observing recurrent occurrences of

569 the same multiple merger events at different locations on the genome, while being aware  
570 of true multiple merger events from rapid successive binary mergers. We believe that  
571 our results pave the way towards the interpretability of GNN and deep learning methods  
572 applied to population genetics. [For further theoretical insights into recent descriptions](#)  
573 [of multiple merger we would like to point the reader towards \[24\].](#)

574 When applying both approaches to simulated sequence data (and not to true ARGs),  
575 both approaches behave differently. *GNNcoal* is not capable to accurately infer model  
576 parameters, ~~i.e.~~ *i.e.* past variation of population size or  $\alpha$ . In contrast, *SM $\beta$ C* ~~performed~~  
577 [performed](#) better than *GNNcoal* when dealing with sequence data (and not true ARG).  
578 *SM $\beta$ C* is capable of recovering  $\alpha$  and the shape of the demographic scenario in recent  
579 times irrespective of whether sequence data or ARG inferred by ARGweaver is given  
580 as input. This is most likely because the statistic used by *SM $\beta$ C* (*i.e.* first coalescent  
581 event in discrete time) is coarser than the statistic used by *GNNcoal* (*i.e.* the exact  
582 ARG). We therefore speculate that the theoretical framework of the *SM $\beta$ C*, although  
583 being in theory less accurate than *GNNcoal*, is more robust and suited for application  
584 to sequence data. More specifically, the issue being faced by the *GNNcoal* is known  
585 as out-of-distribution inference [41], which requires the network to generalize over an  
586 untrained data distribution. This issue happens because *GNNcoal* is not trained using  
587 ARG inferred by ARGweaver. Building a training data set for *GNNcoal* to overcome  
588 this issue is currently impractical due to the inference speed of ARGweaver. However,  
589 future work will aim at increasing robustness of GNN inferences, for instance by adding  
590 uncertainty or multiple models during the training process. Improving the performance of  
591 *GNNcoal* on sequence data requires more efficient and accurate ARG inference methods ~~(~~  
592 ~~which can be used~~, [such as to incorporate inferred \(non-exact\) genealogies into the](#)  
593 [training, thereby accounting for inference errors and for the evaluation of the algorithm](#)  
594 [on a broader spectrum of data sets.](#) ~~The latter common population genetic research~~  
595 [questions. The former](#) observation is important to avoid bias from potential hypothesis  
596 violations of the chosen ARG inference approach).

597 Past demographic history, reproductive mechanisms, and natural selection are among  
598 the major forces driving genome evolution [43]. Hence, in the second part of this  
599 manuscript we focus on integrating selection in both approaches. Currently, no method  
600 (especially if relying only on SFS information) can account for the presence of selection,  
601 linkage [disequilibrium](#), non-constant population size and multiple merger events [43] al-  
602 though recent theoretical framework might render this possible in the future [1].  
603 As a first step to fill this gap, we demonstrate that *GNNcoal* can be used for model  
604 selection to reduce the number of hypotheses to test. Determining which evolutionary  
605 forces are driving the genome evolution is key, as only under the appropriate neutral  
606 population model results of past demography and selection scans can be correctly inter-  
607 preted [43, 45]. The high accuracy of *GNNcoal* in model selection is promising, especially  
608 as other methods based on the SFS alone [56, 46] have limits in presence of complex  
609 demographic scenarios. GNN can possibly overcome these limits, as it is easier to scale  
610 the GNN to estimate more parameters. We follow a thread of previous work [76, 38, 11],  
611 by integrating and recovering selection, multiple merger and population size variation  
612 by simply allowing each fixed region in the genome to have its own  $\alpha$  parameter. In  
613 presence of strong selection, we find lower  $\alpha$  value around the selected loci and high  $\alpha$   
614 value in neutral neighbouring regions. [Hence, our results point out that strong selection](#)

615 can indeed be modeled as a local multiple merger event (see [26, 11, 76]). In presence of  
616 weak selection, no effect on the estimated  $\alpha$  value is observed, demonstrating that weak  
617 selection can be modeled by a binary merger and has only a local effect on the branch  
618 length by shortening it. ~~Hence, our results point out that strong selection can indeed be~~  
619 ~~modeled as a local multiple merger event (see [26, 11, 76])~~. In theory, both approaches  
620 should be able to infer the global  $\alpha$  parameter linked to the reproductive mechanism,  
621 as well as the local  $\alpha$  parameter resulting from selection jointly with the variation of  
622 population size. However, the absence of a simulator capable of simulating data with  
623 selection and non-constant population size under a  $\beta$ -coalescent model prevents us from  
624 delivering such proofs. We show strong evidence that under neutrality our approaches can  
625 recover a constant (and correct)  $\alpha$  along the genome as well as the past variation of the  
626 population size. We further predict that, while selective processes ~~favor coding regions~~  
627 may preferentially occur in coding regions or regulatory potentially non-coding regions,  
628 local variations in  $\alpha$  (as a consequence of sweepstake events) should be indifferent to  
629 the genomic functionality (coding or non-coding regions). Hence, we suggest that current  
630 sequence simulators [7, 35] could be extended to include the aforementioned factors and  
631 *de facto* facilitate the development of machine learning approaches.

632 Our study is unique in developing a ~~new~~-state-of-the-art SMC approach and demon-  
633 strating that computational and mathematical problems can be overcome by deep learn-  
634 ing (here GNN) approaches. The *GNNcoal* approach is, in principle, not limited to the  
635  $\beta$ -coalescent, and should work for other multiple merger models (*e.g.*, Dirac coalescents  
636 [27]) with the appropriate training. Furthermore, our *SM $\beta$ C* approach is the first step to  
637 build a full genome method with an underlying model accounting for positive selection.  
638 In the future, further implementations may be added for a more realistic approach. The  $\alpha$   
639 parameter should be varying along the genome (as a hidden state), as the recombination  
640 rate in the iSMC [5]. This would allow to account for the local effect of strong and weak  
641 selection [1]. The effect of the  $\alpha$  parameter could be also changing through time to better  
642 model the non uniform occurrence of multiple merger events through time. Although  
643 it is mathematically correct to have  $\alpha$  as a constant in time, it is erroneous in practice  
644 (Figure 2 in S1S2). We speculate that those additional features will allow to accurately  
645 model and infer multiple merger events, variation of population size, and selection at each  
646 position on the genome. We believe that deep learning approaches could also be improved  
647 to recover more complex scenarios, providing in depth development on the structure of  
648 the graph neural networks, for example, by accounting for more features. At last, further  
649 investigation are required to make progress in the interpretability of the GNN methods,  
650 namely which statistics and convolution of statistics are used by *GNNcoal* to infer which  
651 parameters.

652 As our approaches are the first of their kind, we chose to restrain our study to haploid  
653 models of  $\beta$  and Kingman coalescent as a proof of principle. However, the *GNNcoal* and  
654 *SM $\beta$ C* approaches can be extended to higher ploidy levels. Diploid versions of the haploid  
655 reproduction models whose genealogies are given by the  $\beta$ -coalescent lead to slightly  
656 different MMC coalescent models which can exhibit simultaneous multiple mergers [8, 10].  
657 Thus, our GNN approach should be directly applicable when trained on these diploid  
658 models which are implemented in *msprime* [7]. However, to adjust the *SM $\beta$ C* approach  
659 would be somewhat more cumbersome (but doable), since we would need to extend the  
660 underlying HMM to account for simultaneous multiple mergers. We emphasise that

661 while there is growing evidence that MMC models produce better fitting genealogies for  
 662 various species [32], there is ongoing discussions about which mathematical models are  
 663 better suited to which species (for example see [3] for cod). We advocate that the life-  
 664 cycle and various ecological factors determine whether a haploid or diploid MMC model  
 665 can be chosen. On the one hand, a diploid MMC model is likely realistic if the species  
 666 has a diploid life-cycle and balanced sex-ratio, so that multiple merger events do indeed  
 667 happen in both sexes. On the other hand, if species are mostly haploid or clonal/asexual  
 668 during their life-cycle (with periodically one short diploid phase for sexual reproduction)  
 669 or exhibit strongly imbalanced sex-ratio, a haploid MMC model may be better suited.  
 670 In their current form, our approaches are applicable to data from species with the latter  
 671 characteristics such as many fungal and micro-parasites of plants and animals (including  
 672 humans) as well as invertebrates (*e.g.* *Daphnia* or aphids) which undergo several clonal  
 673 or parthenogenetic phases of reproduction (and one short sexual phase) per year. This  
 674 represents a non-negligible set of study organisms which are of importance for medicine  
 675 and agriculture [92].

676 Our results on inferred ARGs stress the need for improving ARG inference [15].  
 677 Thanks to the SMC we are close to model the ARG allowing to infer demographic his-  
 678 tory, selection and specific reproductive mechanism. Moreover, the comparison of deep  
 679 learning approaches with model driven *ad hoc* SMC methods may have the potential to  
 680 help us solve ongoing challenges in the field. These include simultaneously inferring and  
 681 accounting for recombination, variation of population size, different type of selection,  
 682 population structure and the variation of the mutation and recombination rate along  
 683 the genome. These issues have puzzled theoreticians and statisticians since the dawn of  
 684 population genetics [43].

685 On a final note, as environmental changes hit us all, we suggest that decreasing the  
 686 computer and power resources needed to perform DL/ GNN analyses should be attempted  
 687 [80]. Based on our study, we suggest that population genetics DL methods could be built  
 688 as a two step process: 1) inferring ARGs, and 2) inferring demography and selection based  
 689 on the ARGs. We speculate that general training sets based on ARGs could be build and  
 690 be widely applicable for inference across many species with different life cycles and life  
 691 history traits, while the inference of ARGs could be undertaken by complementary deep  
 692 learning or Hidden Markov methods.

## 693 Tables

scenario	True $\alpha$	$\alpha$ :SM $\beta$ C,M=3	$\alpha$ :SM $\beta$ C,M=4	$\alpha$ : GNN, M=3	$\alpha$ : GNN, M=10
Constant	2	1.97 (0.005)	1.97 (0.008)	1.99 (0.002)	1.99 (0.003)
Sawtooth	2	1.94 (0.017)	1.87 (0.019)	1.99 (0.002)	1.99 (0.003)
Bottleneck	2	1.97 (0.01)	1.97 (0.009)	1.99 (0.003)	1.99 (0.004)
Decrease	2	1.97 (0.007)	1.97 (0.008)	1.99 (0.003)	1.99 (0.004)
Increase	2	1.97 (0.007)	1.97 (0.008)	1.99 (0.004)	1.99 (0.002)

Table 1: Average estimated values of  $\alpha$  by SM $\beta$ C and GNN $coal$  over ten repetitions under the Kingman coalescent using 10 haploid sequences of 10 Mb and  $\mu = r = 10^{-8}$  per generation per bp. The standard deviation is indicated in brackets.

scenario	True $\alpha$	$\alpha^*$ :SM $\beta$ C,M=3
Constant	1.9	1.86 (0.16)
Bottleneck	1.9	1.89 (0.09)
Increase	1.9	1.93 (0.07)
Decrease	1.9	1.96 (0.04)
Sawtooth	1.9	1.76 (0.17)
Constant	1.7	1.82 (0.10)
Bottleneck	1.7	1.64 (0.23)
Increase	1.7	1.82 (0.10)
Decrease	1.7	1.89 (0.13)
Sawtooth	1.7	1.71 (0.27)
Constant	1.5	1.52 (0.30)
Bottleneck	1.5	1.64 (0.33)
Increase	1.5	1.57 (0.24)
Decrease	1.5	1.60 (0.18)
Sawtooth	1.5	1.66 (0.14)
Constant	1.3	1.31 (0.20)
Bottleneck	1.3	1.2 (0.17)
Increase	1.3	1.24 (0.13)
Decrease	1.3	1.57 (0.11)
Sawtooth	1.3	1.37 (0.16)

Table 2: Average estimated  $\alpha$  values by SM $\beta$ C on simulated sequence data over ten repetitions using 10 sequences of 10 Mb with recombination and mutation rate set to  $1 \times 10^{-8}$  for  $\alpha$  1.9 and 1.7,  $1 \times 10^{-7}$  for  $\alpha$  1.5 and  $1 \times 10^{-6}$  for  $\alpha$  1.3 per generation per bp under a Beta coalescent process. The analysis are run on five different demographic scenarios (Constant population size, Bottleneck, Sudden increase, Sudden decrease and a Sawtooth demography).

## 694 Data availability

695 Code used to generate the simulated data for analysis, training and validation alongside  
696 (trained) deep learning models can be found at [https://github.com/kevinkorfmann/](https://github.com/kevinkorfmann/GNNcoal)  
697 [GNNcoal](https://github.com/kevinkorfmann/GNNcoal) and <https://github.com/kevinkorfmann/GNNcoal-analysis>. Code for SMC  
698 approaches used in this manuscript are available in the R package eSMC2 [https://](https://github.com/TPPSellinger/eSMC2)  
699 [github.com/TPPSellinger/eSMC2](https://github.com/TPPSellinger/eSMC2).

## 700 Acknowledgments

701 This work was supported by the BMBF-funded de.NBI Cloud within the German Network  
702 for Bioinformatics Infrastructure (de.NBI) (031A532B, 031A533A, 031A533B, 031A534A,  
703 031A535A, 031A537A, 031A537B, 031A537C, 031A537D, 031A538A). KK is supported  
704 by a grant from the Deutsche Forschungsgemeinschaft (DFG) through the TUM Interna-  
705 tional Graduate School of Science and Engineering (IGSSE), GSC 81, within the project  
706 GENOMIE QADOP. TS is supported by the Austrian Science Fund (project no. TAI 151-  
707 B). AT acknowledges funding from the DFG grant TE809/1-4 (project 254587930) and  
708 TE809/7-1 (project 317616126). FF and AT acknowledge funding from the DFG Priority  
709 Program SPP1590 on "Probabilistic Structures in Evolution". MF and AT acknowledge  
710 the support from the Imperial College - TUM Partnership award.

## 711 Competing interests

712 The authors declare that no competing interests exist.



## References

- 713
- 714 [1] Frederic Alberti, Carolin Herrmann, and Ellen Baake. Selection, recombination,  
715 and the ancestral initiation graph. *THEORETICAL POPULATION BIOLOGY*,  
716 142:46–56, DEC 2021.
- 717 [2] Einar Arnason and Katrin Halldorsdottir. Nucleotide variation and balancing se-  
718 lection at the Ckma gene in Atlantic cod: analysis with multiple merger coalescent  
719 models. *PEERJ*, 3, FEB 24 2015.
- 720 [3] Einar Árnason, Jere Koskela, Katrín Halldórsdóttir, and Bjarki Eldon. Sweepstakes  
721 reproductive success via pervasive and recurrent selective sweeps. *Elife*, 12:e80781,  
722 2023.
- 723 [4] Gustavo V. Barroso and Julien Y. Dutheil. Mutation rate variation shapes genome-  
724 wide diversity in *Drosophila melanogaster*. preprint, Evolutionary Biology, Septem-  
725 ber 2021.
- 726 [5] Gustavo V. Barroso, Natasa Puzovic, and Julien Y. Dutheil. Inference of recombi-  
727 nation maps from a single pair of genomes and its application to ancient samples.  
728 *PLOS Genetics*, 15(11), NOV 2019.
- 729 [6] CJ Battey, Peter L Ralph, and Andrew D Kern. Predicting geographic location  
730 from genetic variation with deep neural networks. *eLife*, 9:e54507, June 2020.
- 731 [7] Franz Baumdicker, Gertjan Bisschop, Daniel Goldstein, Graham Gower, Aaron P.  
732 Ragsdale, Georgia Tsambos, Sha Zhu, Bjarki Eldon, E. Castedo Ellerman, Jared G.  
733 Galloway, Ariella L. Gladstein, Gregor Gorjanc, Bing Guo, Ben Jeffery, Warren W.  
734 Kretzschumar, Konrad Lohse, Michael Matschiner, Dominic Nelson, Nathaniel S.  
735 Pope, Consuelo D. Quinto-Cortes, Murillo F. Rodrigues, Kumar Saunack, Thibaut  
736 Sellinger, Kevin Thornton, Hugo van Kemenade, Anthony W. Wohns, Yan Wong,  
737 Simon Gravel, Andrew D. Kern, Jere Koskela, Peter L. Ralph, and Jerome Kelleher.  
738 Efficient ancestry and mutation simulation with msprime 1.0. *GENETICS*, 220(3),  
739 MAR 3 2022.
- 740 [8] Matthias Birkner, Jochen Blath, and Bjarki Eldon. An Ancestral Recombina-  
741 tion Graph for Diploid Populations with Skewed Offspring Distribution. *Genetics*,  
742 193(1):255–290, JAN 2013.
- 743 [9] Matthias Birkner, Jochen Blath, Martin Moehle, Matthias Steinruecken, and Jo-  
744 hanna Tams. A modified lookdown construction for the Xi-Fleming-Viot process  
745 with mutation and populations with recurrent bottlenecks. *arXiv:0808.0412*, 2008.
- 746 [10] Matthias Birkner, Huili Liu, and Anja Sturm. Coalescent results for diploid ex-  
747 changeable population models I. *Electronic Journal of Probability*, 23, 2018.
- 748 [11] Gertjan Bisschop, Konrad Lohse, and Derek Setter. Sweeps in time: leveraging the  
749 joint distribution of branch lengths. *GENETICS*, 219(2), OCT 2021.
- 750 [12] Jochen Blath, Adrian Gonzalez Casanova, Noemi Kurt, and Maite Wilke-  
751 Berenguer. The seed bank coalescent with simultaneous switching. *Electronic*  
752 *Journal of Probability*, 25, 2020.

- 753 [13] Simon Boitard, Willy Rodríguez, Flora Jay, Stefano Mona, and Frédéric Austerlitz.  
754 Inferring population size history from large samples of genome-wide molecular data  
755 - an approximate bayesian computation approach. 12(3):e1005877.
- 756 [14] Erwin Bolthausen and A-S Sznitman. On ruelle’s probability cascades and an  
757 abstract cavity method. *Communications in mathematical physics*, 197(2):247–276,  
758 1998.
- 759 [15] Debora Y. C. Brandt, Xinzhu Wei, Yun Deng, Andrew H. Vaughn, and Rasmus  
760 Nielsen. Evaluation of methods for estimating coalescence times using ancestral  
761 recombination graphs. *GENETICS*, 221(1), MAY 5 2022.
- 762 [16] Michael M. Bronstein, Joan Bruna, Yann LeCun, Arthur Szlam, and Pierre Van-  
763 dergheynst. Geometric deep learning: Going beyond euclidean data. *IEEE Signal*  
764 *Processing Magazine*, 34(4):18–42, jul 2017.
- 765 [17] E. Brunet, B. Derrida, A. H. Mueller, and S. Munier. Noisy traveling waves: Effect  
766 of selection on genealogies. *Europhysics Letters*, 76(1):1–7, OCT 2006.
- 767 [18] E. Brunet, B. Derrida, A. H. Mueller, and S. Munier. Effect of selection on ancestry:  
768 An exactly soluble case and its phenomenological generalization. *Physical Review*  
769 *E*, 76(4, 1), OCT 2007.
- 770 [19] Klara Elisabeth Burger, Peter Pfaffelhuber, and Franz Baumdicker. Neural net-  
771 works for self-adjusting mutation rate estimation when the recombination rate is  
772 unknown. *PLOS Computational Biology*, 18(8):1–17, 08 2022.
- 773 [20] Wenming Cao, Zhiyue Yan, Zhiquan He, and Zhihai He. A comprehensive survey  
774 on geometric deep learning. *IEEE Access*, 8:35929–35949, 2020.
- 775 [21] Adrián González Casanova, Verónica Miró Pina, and Arno Siri-Jégousse. The Sym-  
776 metric Coalescent and Wright-Fisher models with bottlenecks. *arXiv:1903.05642*  
777 *[math]*, September 2020. arXiv: 1903.05642.
- 778 [22] Jianhai Chen, Pan Ni, Xinyun Li, Jianlin Han, Ivan Jakovlic, Chengjun Zhang, and  
779 Shuhong Zhao. Population size may shape the accumulation of functional mutations  
780 following domestication. *BMC Evolutionary Biology*, 18, JAN 19 2018.
- 781 [23] LLOYD Demetrius. Adaptive value, entropy and survivorship curves. *Nature*,  
782 275(5677):213–214, September 1978.
- 783 [24] Dimitrios Diamantidis, Wai-Tong (Louis) Fan, Matthias Birkner, and John Wake-  
784 ley. Bursts of coalescence within population pedigrees whenever big families occur.  
785 October 2023.
- 786 [25] P Donnelly and TG Kurtz. Particle representations for measure-valued population  
787 models. *Annals of Probability*, 27(1):166–205, JAN 1999.
- 788 [26] R Durrett and J Schweinsberg. A coalescent model for the effect of advantageous  
789 mutations on the genealogy of a population. *Stochastic Processes and their Appli-*  
790 *cations*, 115(10):1628–1657, OCT 2005.

- 791 [27] B Eldon and J Wakeley. Coalescent processes when the distribution of offspring  
792 number among individuals is highly skewed. *Genetics*, 172(4):2621–2633, APR  
793 2006.
- 794 [28] Bjarki Eldon, Matthias Birkner, Jochen Blath, and Fabian Freund. Can the Site-  
795 Frequency Spectrum Distinguish Exponential Population Growth from Multiple-  
796 Merger Coalescents? *Genetics*, 199(3):841+, MAR 2015.
- 797 [29] Malaspinas et al. A genomic history of Aboriginal Australia. *Nature*,  
798 538(7624):207+, OCT 13 2016.
- 799 [30] Matthias Fey and Jan Eric Lenssen. Fast graph representation learning with Py-  
800 Torch geometric.
- 801 [31] Lex Flagel, Yaniv Brandvain, and Daniel R Schrider. The Unreasonable Effective-  
802 ness of Convolutional Neural Networks in Population Genetic Inference. *Molecular*  
803 *Biology and Evolution*, 36(2):220–238, 12 2018.
- 804 [32] Fabian Freund, Elise Kerdoncuff, Sebastian Matuszewski, Marguerite Lapierre,  
805 Marcel Hildebrandt, Jeffrey D. Jensen, Luca Ferretti, Amaury Lambert, Timo-  
806 thy B. Sackton, and Guillaume Achaz. Interpreting the pervasive observation of  
807 U-shaped Site Frequency Spectra. preprint, *Evolutionary Biology*, April 2022.
- 808 [33] L. M. Gattepaille, M. Jakobsson, and M. G. B. Blum. Inferring population size  
809 changes with sequence and SNP data: lessons from human bottlenecks. *Heredity*,  
810 110(5):409–419, MAY 2013.
- 811 [34] Lucie Gattepaille, Torsten Günther, and Mattias Jakobsson. Inferring Past Effective  
812 Population Size from Distributions of Coalescent Times. *Genetics*, 204(3):1191–  
813 1206, November 2016.
- 814 [35] Benjamin C. Haller, Jared Galloway, Jerome Kelleher, Philipp W. Messer, and  
815 Peter L. Ralph. Tree-sequence recording in slim opens new horizons for forward-time  
816 simulation of whole genomes. *MOLECULAR ECOLOGY RESOURCES*, 19(2):552–  
817 566, MAR 2019.
- 818 [36] Rebecca B. Harris and Jeffrey D. Jensen. Considering genomic scans for selection as  
819 coalescent model choice. *GENOME BIOLOGY AND EVOLUTION*, 12(6):871–877,  
820 JUN 2020.
- 821 [37] Dennis Hedgecock and Alexander I. Pudovkin. Sweepstakes reproductive success  
822 in highly fecund marine fish and shellfish: a review and Commentary. *Bulletin of*  
823 *Marine Science*, 87(4):971–1002, OCT 2011.
- 824 [38] Hussein A. Hejase, Ziyi Mo, Leonardo Campagna, and Adam Siepel. A deep-  
825 learning approach for inference of selective sweeps from the ancestral recombination  
826 graph. *MOLECULAR BIOLOGY AND EVOLUTION*, 39(1), JAN 7 2022.
- 827 [39] Melissa Hubisz and Adam Siepel. Inference of ancestral recombination graphs using  
828 argweaver. In JY Dutheil, editor, *STATISTICAL POPULATION GENOMICS*,  
829 volume 2090 of *Methods in Molecular Biology*, pages 231–266. 2020.

- 830 [40] RR HUDSON. Properties of a neutral allele model with intragenic recombination.  
831 *Theoretical Population Biology*, 23(2):183–201, 1983.
- 832 [41] Eyke Hüllermeier and Willem Waegeman. Aleatoric and epistemic uncertainty in  
833 machine learning: an introduction to concepts and methods. *Machine Learning*,  
834 110(3):457–506, March 2021.
- 835 [42] Ulas Isildak, Alessandro Stella, and Matteo Fumagalli. Distinguishing between re-  
836 cent balancing selection and incomplete sweep using deep neural networks. *Molec-  
837 ular Ecology Resources*, 21(8):2706–2718, November 2021.
- 838 [43] Parul Johri, Charles F. Aquadro, Mark Beaumont, Brian Charlesworth, Laurent  
839 Excoffier, Adam Eyre-Walker, Peter D. Keightley, Michael Lynch, Gil McVean,  
840 Bret A. Payseur, Susanne P. Pfeifer, Wolfgang Stephan, and Jeffrey D. Jensen.  
841 Recommendations for improving statistical inference in population genomics. *PLOS  
842 Biology*, 20(5):e3001669, May 2022.
- 843 [44] Parul Johri, Brian Charlesworth, and Jeffrey D. Jensen. Toward an evolutionar-  
844 ily appropriate null model: Jointly inferring demography and purifying selection.  
845 *GENETICS*, 215(1):173–192, MAY 2020.
- 846 [45] Parul Johri, Kellen Riall, Hannes Becher, Laurent Excoffier, Brian Charlesworth,  
847 and Jeffrey D. Jensen. The impact of purifying and background selection on the in-  
848 ference of population history: Problems and prospects. *MOLECULAR BIOLOGY  
849 AND EVOLUTION*, 38(7):2986–3003, JUL 2021.
- 850 [46] Mamoru Kato, Daniel A. Vasco, Ryuichi Sugino, Daichi Narushima, and Alexander  
851 Krasnitz. Sweepstake evolution revealed by population-genetic analysis of copy-  
852 number alterations in single genomes of breast cancer. *Royal Society of Open Sci-  
853 ence*, 4(9), SEP 2017.
- 854 [47] Jerome Kelleher, Kevin R. Thornton, Jaime Ashander, and Peter L. Ralph. Efficient  
855 pedigree recording for fast population genetics simulation. 14(11):e1006581.
- 856 [48] Jerome Kelleher, Yan Wong, Anthony W. Wohns, Chaimaa Fadil, Patrick K.  
857 Albers, and Gil McVean. Inferring whole-genome histories in large population  
858 datasets. *Nature Genetics*, 51(9):1330–1338, September 2019.
- 859 [49] Jerome Kelleher, Yan Wong, Anthony W. Wohns, Chaimaa Fadil, Patrick K. Al-  
860 bers, and Gil McVean. Inferring whole-genome histories in large population datasets  
861 (vol 51, pg 1330, 2019). *Nature Genetics*, 51(11):1660, NOV 2019.
- 862 [50] Caleb Ki and Jonathan Terhorst. Exact decoding of the sequentially Markov coa-  
863 lescent, September 2020.
- 864 [51] Younhun Kim, Frederic Koehler, Ankur Moitra, Elchanan Mossel, and Govind  
865 Ramnarayan. How Many Subpopulations Is Too Many? Exponential Lower Bounds  
866 for Inferring Population Histories. *Journal of Computational Biology*, 27(4):613–  
867 625, APR 1 2020.
- 868 [52] JFC Kingman. The Coalescent . *Stochastic Processes and their Applications*, 13,  
869 1982.

- 870 [53] Thomas N. Kipf and Max Welling. Semi-Supervised Classification with Graph  
871 Convolutional Networks. 2016.
- 872 [54] Kevin Korfmann, Oscar E Gaggiotti, and Matteo Fumagalli. Deep Learning in Pop-  
873 ulation Genetics. *Genome Biology and Evolution*, 15(2):evad008, February 2023.
- 874 [55] Jere Koskela. Multi-locus data distinguishes between population growth and mul-  
875 tiple merger coalescents. *STATISTICAL APPLICATIONS IN GENETICS AND*  
876 *MOLECULAR BIOLOGY*, 17(3), JUN 2018.
- 877 [56] Jere Koskela and Maite Wilke Berenguer. Robust model selection between popula-  
878 tion growth and multiple merger coalescents. *Mathematical Biosciences*, 311:1–12,  
879 MAY 2019.
- 880 [57] John Boaz Lee, Ryan Rossi, and Xiangnan Kong. Graph Classification using Struc-  
881 tural Attention. In *Proceedings of the 24th ACM SIGKDD International Conference*  
882 *on Knowledge Discovery & Data Mining*, pages 1666–1674, London United King-  
883 dom, July 2018. ACM.
- 884 [58] Heng Li and Richard Durbin. Inference of human population history from individual  
885 whole-genome sequences. *Nature*, 475(7357):493–U84, JUL 28 2011.
- 886 [59] Ali Mahmoudi, Jere Koskela, Jerome Kelleher, Yao-ban Chan, and David Balding.  
887 Bayesian inference of ancestral recombination graphs. *PLOS COMPUTATIONAL*  
888 *BIOLOGY*, 18(3), MAR 2022.
- 889 [60] P Marjoram and JD Wall. Fast “coalescent” simulation. *BMC Genetics*, 7, MAR  
890 15 2006.
- 891 [61] Sebastian Matuszewski, Marcel E. Hildebrandt, Guillaume Achaz, and Jeffrey D.  
892 Jensen. Coalescent processes with skewed offspring distributions and non-  
893 equilibrium demography. *Genetics*, 2017.
- 894 [62] GAT McVean and NJ Cardin. Approximating the coalescent with recombina-  
895 tion. *Philosophical Transactions of the Royal Society B-Biological Sciences*,  
896 360(1459):1387–1393, JUL 29 2005.
- 897 [63] F Menardo, S Gagneux, and F Freund. Multiple merger genealogies in outbreaks of  
898 *Mycobacterium tuberculosis*. *Molecular Biology and Evolution*, 07 2020. msaa179.
- 899 [64] Alistair Miles, pyup io bot, Murillo R, Peter Ralph, Nick Harding, Rahul Pisupati,  
900 Summer Rae, and Tim Millar. cggh/scikit-allel: v1.3.3.
- 901 [65] M Mohle and S Sagitov. A classification of coalescent processes for haploid ex-  
902 changeable population models. *Annals of Probability*, 29(4):1547–1562, OCT 2001.
- 903 [66] Ana Y. Morales-Arce, Rebecca B. Harris, Anne C. Stone, and Jeffrey D. Jensen.  
904 Evaluating the contributions of purifying selection and progeny-skew in dictat-  
905 ing within-host *Mycobacterium tuberculosis* evolution. *Evolution*, 74(5):992–1001,  
906 MAY 2020.

- 907 [67] Richard A. Neher and Oskar Hallatschek. Genealogies of rapidly adapting popula-  
908 tions. *Proceedings of the National Academy of Sciences*, 110(2):437–442, January  
909 2013.
- 910 [68] Dominic Nelson, Jerome Kelleher, Aaron P. Ragsdale, Claudia Moreau, Gil  
911 McVean, and Simon Gravel. Accounting for long-range correlations in genome-  
912 wide simulations of large cohorts. *PLOS Genetics*, 16(5), MAY 2020.
- 913 [69] Hiro-Sato Niwa, Kazuya Nashida, and Takashi Yanagimoto. Reproductive skew in  
914 japanese sardine inferred from dna sequences. *ICES Journal of Marine Science*,  
915 73(9):2181–2189, 2016.
- 916 [70] Adam Paszke, Sam Gross, Soumith Chintala, Gregory Chanan, Edward Yang,  
917 Zachary DeVito, Zeming Lin, Alban Desmaison, Luca Antiga, and Adam Lerer.  
918 Automatic differentiation in PyTorch. October 2017.
- 919 [71] J Pitman. Coalescents with multiple collisions. *Annals of Probability*, 27(4):1870–  
920 1902, OCT 1999.
- 921 [72] Xinghu Qin, Charleston W. K. Chiang, and Oscar E. Gaggiotti. Deciphering sig-  
922 natures of natural selection via deep learning. *bioRxiv*, 2021.
- 923 [73] Matthew D. Rasmussen, Melissa J. Hubisz, Ilan Gronau, and Adam Siepel.  
924 Genome-wide inference of ancestral recombination graphs. *PLOS GENETICS*,  
925 10(5), MAY 2014.
- 926 [74] Daniel P Rice, John Novembre, and Michael M Desai. Distinguishing multiple-  
927 merger from kingman coalescence using two-site frequency spectra. *bioRxiv*, 2018.
- 928 [75] Alan R. Rogers and Chad Huff. Linkage disequilibrium between loci with unknown  
929 phase. 182(3):839–844.
- 930 [76] Andrew M. Sackman, Rebecca B. Harris, and Jeffrey D. Jensen. Inferring demog-  
931 raphy and selection in organisms characterized by skewed offspring distributions.  
932 *GENETICS*, 211(3):1019–1028, MAR 2019.
- 933 [77] S Sagitov. The general coalescent with asynchronous mergers of ancestral lines.  
934 *Journal of Applied Probability*, 36(4):1116–1125, DEC 1999.
- 935 [78] S Sagitov. Convergence to the coalescent with simultaneous multiple mergers. *Jour-  
936 nal of Applied Probability*, 40(4):839–854, DEC 2003.
- 937 [79] Théophile Sanchez, Jean Cury, Guillaume Charpiat, and Flora Jay. Deep learning  
938 for population size history inference: Design, comparison and combination with  
939 approximate bayesian computation. 21(8):2645–2660.
- 940 [80] Nicolae Sapoval, Amirali Aghazadeh, Michael G. Nute, Dinler A. Antunes, Advait  
941 Balaji, Richard Baraniuk, C. J. Barberan, Ruth Dannenfelser, Chen Dun, Mo-  
942 hammadamin Edrisi, R. A. Leo Elworth, Bryce Kille, Anastasios Kyriallidis, Luay  
943 Nakhleh, Cameron R. Wolfe, Zhi Yan, Vicky Yao, and Todd J. Treangen. Cur-  
944 rent progress and open challenges for applying deep learning across the biosciences.  
945 *Nature Communications*, 13(1):1728, December 2022.

- 946 [81] Ori Sargsyan and John Wakeley. A coalescent process with simultaneous multiple  
947 mergers for approximating the gene genealogies of many marine organisms. *Theo-*  
948 *retical population biology*, 74(1):104–114, 2008.
- 949 [82] Stephan Schiffels and Richard Durbin. Inferring human population size and sep-  
950 aration history from multiple genome sequences. *Nature Genetics*, 46(8):919–925,  
951 AUG 2014.
- 952 [83] Michael Schlichtkrull, Thomas N. Kipf, Peter Bloem, Rianne van den Berg, Ivan  
953 Titov, and Max Welling. Modeling relational data with graph convolutional net-  
954 works, 2017.
- 955 [84] J Schweinsberg. Coalescent processes obtained from supercritical Galton-Watson  
956 processes. *Stochastic Processes and their Applications*, 106(1):107–139, JUL 2003.
- 957 [85] Thibaut Paul Patrick Sellinger, Diala Abu Awad, Markus Moest, and Aurelien  
958 Tellier. Inference of past demography, dormancy and self-fertilization rates from  
959 whole genome sequence data. *PLOS Genetics*, 16(4), APR 2020.
- 960 [86] Thibaut Paul Patrick Sellinger, Diala Abu-Awad, and Aurelien Tellier. Limits and  
961 convergence properties of the sequentially markovian coalescent. *MOLECULAR*  
962 *ECOLOGY RESOURCES*, 21(7):2231–2248, OCT 2021.
- 963 [87] Sara Sheehan and Yun S. Song. Deep Learning for Population Genetic Inference.  
964 *PLOS Computational Biology*, 12(3), MAR 2016.
- 965 [88] Leo Speidel, Marie Forest, Sinan Shi, and Simon R. Myers. A method for genome-  
966 wide genealogy estimation for thousands of samples. *Nature Genetics*, 51(9):1321+,  
967 SEP 2019.
- 968 [89] Matthias Steinruecken, Matthias Birkner, and Jochen Blath. Analysis of DNA  
969 sequence variation within marine species using Beta-coalescents. *Theoretical Pop-*  
970 *ulation Biology*, 87:15–24, AUG 2013.
- 971 [90] Wolfgang Stephan. Selective Sweeps. *Genetics*, 211(1):5–13, January 2019.
- 972 [91] Stefan Struett, Thibaut Sellinger, Sylvain Glémin, Aurélien Tellier, and Stefan Lau-  
973 rent. Inference of evolutionary transitions to self-fertilization using whole-genome  
974 sequences. *bioRxiv*, 2022.
- 975 [92] Aurelien Tellier and Christophe Lemaire. Coalescence 2.0: a multiple branch-  
976 ing of recent theoretical developments and their applications. *Molecular Ecology*,  
977 23(11):2637–2652, JUN 2014.
- 978 [93] Jonathan Terhorst, John A. Kamm, and Yun S. Song. Robust and scalable inference  
979 of population history froth hundreds of unphased whole genomes. *Nature Genetics*,  
980 49(2):303–309, FEB 2017.
- 981 [94] Gautam Upadhyya and Matthias Steinrücken. Robust Inference of Population Size  
982 Histories from Genomic Sequencing Data. preprint, *Genetics*, May 2021.

- 983 [95] Ke Wang, Iain Mathieson, Jared O’Connell, and Stephan Schiffels. Tracking human  
984 population structure through time from whole genome sequences. *PLOS Genetics*,  
985 16(3), MAR 2020.
- 986 [96] Zhanpeng Wang, Jiaping Wang, Michael Kourakos, Nhung Hoang, Hyong Hark  
987 Lee, Iain Mathieson, and Sara Mathieson. Automatic inference of demographic  
988 parameters using generative adversarial networks. *Molecular Ecology Resources*,  
989 21(8):2689–2705, 2021.
- 990 [97] Peter R. Wilton, Shai Carmi, and Asger Hobolth. The SMC’ Is a Highly Accurate  
991 Approximation to the Ancestral Recombination Graph. *Molecular Biology and*  
992 *Evolution*, 200(1):343–U637, MAY 2015.
- 993 [98] C Wiuf and J Hein. Recombination as a point process along sequences. *Theoretical*  
994 *Population Biology*, 55(3):248–259, JUN 1999.
- 995 [99] Keyulu Xu, Weihua Hu, Jure Leskovec, and Stefanie Jegelka. How powerful are  
996 graph neural networks? In *International Conference on Learning Representations*,  
997 2019.
- 998 [100] Zhilin Yang, William W. Cohen, and Ruslan Salakhutdinov. Revisiting semi-  
999 supervised learning with graph embeddings. *CoRR*, abs/1603.08861, 2016.
- 1000 [101] Burak Yelmen, Aurélien Decelle, Linda Ongaro, Davide Marnetto, Corentin Tallec,  
1001 Francesco Montinaro, Cyril Furtlehner, Luca Pagani, and Flora Jay. Creating artificial  
1002 human genomes using generative neural networks. *PLOS Genetics*, 17(2):1–22,  
1003 02 2021.
- 1004 [102] Rex Ying, Jiaxuan You, Christopher Morris, Xiang Ren, William L. Hamilton,  
1005 and Jure Leskovec. Hierarchical graph representation learning with differentiable  
1006 pooling.
- 1007 [103] Muhan Zhang and Yixin Chen. Link prediction based on graph neural networks. In  
1008 S. Bengio, H. Wallach, H. Larochelle, K. Grauman, N. Cesa-Bianchi, and R. Gar-  
1009 nett, editors, *Advances in Neural Information Processing Systems*, volume 31. Cur-  
1010 ran Associates, Inc., 2018.
- 1011 [104] Jie Zhou, Ganqu Cui, Shengding Hu, Zhengyan Zhang, Cheng Yang, Zhiyuan Liu,  
1012 Lifeng Wang, Changcheng Li, and Maosong Sun. Graph neural networks: A review  
1013 of methods and applications. 1:57–81.